Engineering Structures 291 (2023) 116459

Contents lists available at ScienceDirect

Engineering Structures

journal homepage: www.elsevier.com/locate/engstruct

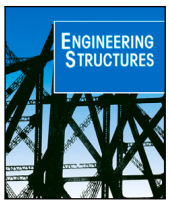

Indirect damage detection for bridges using sensing and temporarily parked vehicles

Zhenkun Li, Yifu Lan, Weiwei Lin *

Department of Civil Engineering, Aalto University, Rakentajanaukio 4 A, 02150 Espoo, Finland

ARTICLE INFO

Keywords:
Structural health monitoring
Damage detection
Indirect method
Contact-point response
Substructure

ABSTRACT

Due to the influence of many factors such as vehicle properties, road roughness, and external noises, accurate indirect identification of the bridge's frequencies is challenging. Further, given the insensitivity of the bridge's frequencies to damage and limited acquired modal information, damage detection is often difficult to be implemented in practical engineering. This paper proposes an indirect approach to localize and quantify bridge damage using sensing and parked vehicles. First, equations for back-calculating residual contact-point responses of the sensing vehicle with suspension and tire damping and sensor-installing errors are newly deduced to eliminate its self-frequencies and suppress the negative effects of road roughness. Second, another temporarily parked truck is introduced to increase the amount of modal information about the bridge and its sensitivity to local damage. Third, a novel modal assurance criterion-based objective function using indirectly identified frequencies is proposed to enhance the robustness of damage detection. Numerical simulations utilizing a half-car model and a simply supported bridge verify the effectiveness of the proposed strategy. It is found that the new objective function improves the robustness of damage detection when the parked truck is employed at different positions. In addition, a higher speed of the sensing vehicle can negatively affect damage detection, while the ongoing traffic can help to resist the negative impact of environmental noises and bridge damping. By considering possible influence factors and model updating errors in practical applications, the damage can be located and quantified with acceptable precision.

1. Introduction

Existing bridge structures are prone to deterioration and exposed to natural hazards and man-made disasters, such as typhoons, floods, earthquakes, car crashes, and ship collisions [1]. In addition, traffic loads have boosted substantially in many countries during the past two decades because of increasing human needs. These external influences are damaging to the safety of the bridge and may expedite the formation of deterioration. To ensure safe operations, it is necessary to promptly detect bridge damage and implement corresponding maintenance measures regularly [2,3]. Damage detection techniques, as the core components in structural health monitoring (SHM), can provide essential ways for bridge condition assessment [4,5]. Conventionally, bridge maintenance requires experienced engineers to inspect the bridge's surface to find possible defects visually. Yet, as the increase in bridge scales and complexity, visual inspection becomes dangerous, labor-intensive, time-consuming, and even unachievable [6]. The vibration-based methodology can bring novel solutions to the aforementioned issues. Typically, these methods rely on structural modal changes before and after damage occurs. Therefore, they are not restricted to surface faults and can be sensitive to interior damage. However, the traditional vibration-based methods generally require a certain number of sensors installed directly on the bridge (named the direct method), which is costly to be applied in practical engineering. Moreover, huge amounts of data will be collected if continuous monitoring is required [7]. As a matter of this fact, monitoring systems are typically installed on large or extremely important bridges. As the number of aging and deteriorating bridges is increasing, there is a pressing need to develop efficient and cost-effective technologies for bridge damage detection.

In 2004, Yang et al. [8] initialized the indirect method for bridge modal parameter identification. The passing vehicle was utilized as an exciter and moving sensor to gather the bridge's vibrations, and its fundamental frequency was successfully identified. The idea was later verified by Lin and Yang [9] in a field test on a 30 m span of the Da-Wu-Lun Bridge. After the two studies, many researchers are attracted by the indirect idea for bridge health monitoring [10–12], and it has been extended to modal shape, damping, and road roughness identifications [13–15]. For indirect frequency identification, as the accelerations

* Corresponding author.
E-mail addresses: zhenkun.li@aalto.fi (Z. Li), yifu.lan@aalto.fi (Y. Lan), weiwei.lin@aalto.fi (W. Lin).

https://doi.org/10.1016/j.engstruct.2023.116459
Received 2 March 2023; Received in revised form 12 May 2023; Accepted 8 June 2023
Available online 17 June 2023

are collected by sensors attached to the vehicle, its frequencies will prevail over the bridge's in the frequency domain. Thus, naturally, a band filter can be used to filter out the vehicle's frequency and highlight the bridge's frequencies [16]. Also, it was found that the time- and frequency-domain signal process tools were much helpful for picking out the bridge frequencies from those of the vehicle [17–20]. However, these methods generally require that the vehicle's frequencies be known beforehand, which is not commonly available in practice.

To remove the influence of the vehicle's self-frequencies, the concept of contact-point (CP) responses is proposed by Yang et al. [21]. As the CP response is merely related to the road roughness and the bridge's vibrations, information about the vehicle is fully eliminated. It was tested that the CP response is superior to generally used original accelerations for indirect bridge information extraction [22–24]. Notwithstanding, the CP response includes the bridge's information and road roughness, but the latter plays a leading role. Aiming at weakening the inverse effects of road roughness, Kong et al. [25] proposed to employ two connected vehicles, and the residual accelerations of the front and rear axles were utilized, which was proved to outperform frequency-domain signal subtraction [26]. Similar techniques are then employed for the CP response of two vehicles [27,28]. Nevertheless, two on-site connected vehicles with the same trace are generally difficult to operate in practical engineering. Therefore, scholars began to focus on using the response of a single vehicle's different axles, and it was verified effective for indirect bridge information identification [29–31]. However, in the existing studies, the damping of vehicle tires and suspensions was not fully considered. Moreover, current research has just explored the identification of bridge frequencies, and few references have investigated the effectiveness of extracted frequencies for some downstream assignments, such as damage detection.

Current approaches for damage detection can generally be split into two categories: model-free and model-based methods [32]. The former requires no parametric model of the structure. The collected signals can be addressed directly to identify the health state of the structure. Typical techniques include empirical mode decomposition, variational mode decomposition, wavelet transform, or data-driven tools such as machine learning to find the key pattern showing the structural damage condition [33–37]. The model-free methods can circumvent the process of building and updating the structural finite element (FE) model. However, it is typically challenging for them to localize the damage, and they are susceptible to surrounding noises. Different from model-free approaches, model-based methods rely on FE models. One or several objective functions are required to minimize the errors between the experimental and built simulated models by model updating. Typically employed characteristics of the structure include natural frequency, modal shapes, frequency response function, modal flexibility, and strain energy [38–41]. The model-based approaches can quantitatively and locationally identify the structural damage. However, due to measurement limitations and the influence of environmental factors, only several modes of the original structure (without physical modifications) can be identified, e.g., first several natural frequencies and modal shapes. It is usually difficult to accurately update the FE model and capture changes due to local damage with limited modes. Therefore, some physical modifications can be introduced to increase the obtained modal information about the structure, such as supports and masses [32,42], which is beneficial to model updating and precise damage identification. It had been verified that the parked vehicle could induce changes in bridge frequencies [43], which was potential for increase the acquired modes of the bridge. In 2018, He and Ren [44] proposed utilizing a parked vehicle at different positions of the bridge to increase its identified modes for damage detection, and the approach was validated by a self-made laboratory vehicle and bridge. Results showed that the decrease of bridge frequencies due to damage could be amplified by introducing the extra parked vehicle. Based on this principle, Cao et al. [45] proposed to identify bridge damage severity using the frequency-parameter change rate (FPCR), and the relationship between damage severity and FPCR of the damaged element was acquired. However, the existing studies typically rely on the impulse excitation on the bridge. Applying such an excitation in practical engineering is difficult and may necessitate traffic stops.

In this paper, a novel damage detection method utilizing two vehicles: a sensing vehicle (SV) and a temporarily parked truck (PT) is proposed. The feasibility of employing indirectly identified frequencies for damage detection, localization, and quantification is investigated. Unlike single-axle or two-axle test vehicles, normal vehicle models for simulating commercial cars are employed, in which the tires and suspensions are considered simultaneously. For better retrieving the bridge's frequencies, the residual CP response of the SV is back-calculated from its accelerations, and the influence of sensor installation positions is discussed in the derived equations. In addition, the PT is employed on different positions of the bridge as a physical modification to improve the sensitivity of the bridge frequency to local damage and increase the amount of modal information about the bridge. During the damage detection process, the SV is regarded as the exciter and signal receiver at the same time for bridge frequency identification. No external forces, such as impulse or harmonic excitations, are required. Further, to enhance the robustness of the model updating, a new objective function based on the modal assurance criterion (MAC) is proposed to improve the sparsity of damage factors, resulting in better damage identification results compared to traditional relative error-based functions. The structure of this paper is as follows: After Section 1, the basic theory for calculating CP responses of the SV and the proposed objective function is introduced in Section 2. Section 3 provides employed parameters of the vehicle bridge interaction (VBI) system, and two case studies are discussed. Section 4 explores more influence factors for real-life applications of the proposed method. Finally, this paper is concluded in Section 5.

2. Theory foundation

2.1. Indirect bridge frequency identification

2.1.1. VBI system

This section introduces the employed VBI system in this paper. They are the sensing vehicle, temporarily parked truck, simply supported bridge, and road roughness of the bridge pavement. Ongoing traffic will be considered and introduced in Section 4.

SV and PT models. The vehicles, bridge, and road roughness are shown in Fig. 1. The SV is assumed to be driven at a constant speed v for indirectly identifying the bridge's frequencies. It is simulated by a two-axle model owing four degrees of freedom (DOFs): body bounce (z_{sv}), body rotation (θ_{sv}), front and rear wheel bounces (z_{t1} and z_{t2}). The SV's body mass and moment of inertia are m_v and I_v, respectively, with the front wheel's mass of m_{t1} and the rear wheel's mass of m_{t2}. The stiffness and damping values of the SV's front and rear suspension system are represented by k_{s1}, c_{s1} and k_{s2}, c_{s2}. Similarly, the tire's stiffness and damping values are k_{t1}, c_{t1} and k_{t2}, c_{t2} for front and rear wheels. The center of gravity of the SV's body is located by a_1 and a_2, and $a = a_1 + a_2$ is the axle distance. Since it is hard to find a vehicle body's center of gravity accurately, we assume that the accelerometer is installed in a position with a distance of e from the center of gravity. The vehicle's body and wheels are assumed as rigid objects, and they have no deformation under the influence of external forces. Based on the proposed SV model, its dynamic equilibrium equations are shown in Eq. (1),

$$\mathbf{M}_{sv}\ddot{\mathbf{z}}_{sv}(t) + \mathbf{C}_{sv}\dot{\mathbf{z}}_{sv}(t) + \mathbf{K}_{sv}\mathbf{z}_{sv}(t) = \boldsymbol{f}_{cv} \tag{1}$$

where $\mathbf{M}_{sv}$, $\mathbf{C}_{sv}$, and $\mathbf{K}_{sv}$ are the SV's mass, damping, and stiffness matrices, and $\ddot{\mathbf{z}}_{sv}(t)$, $\dot{\mathbf{z}}_{sv}(t)$, and $\mathbf{z}_{sv}(t)$ are its accelerations, velocities, and displacements at all four DOFs, as shown in Eq. (2). Vibrations of the SV will change with time t when it passes the bridge. $\boldsymbol{f}_{cv}$ means the

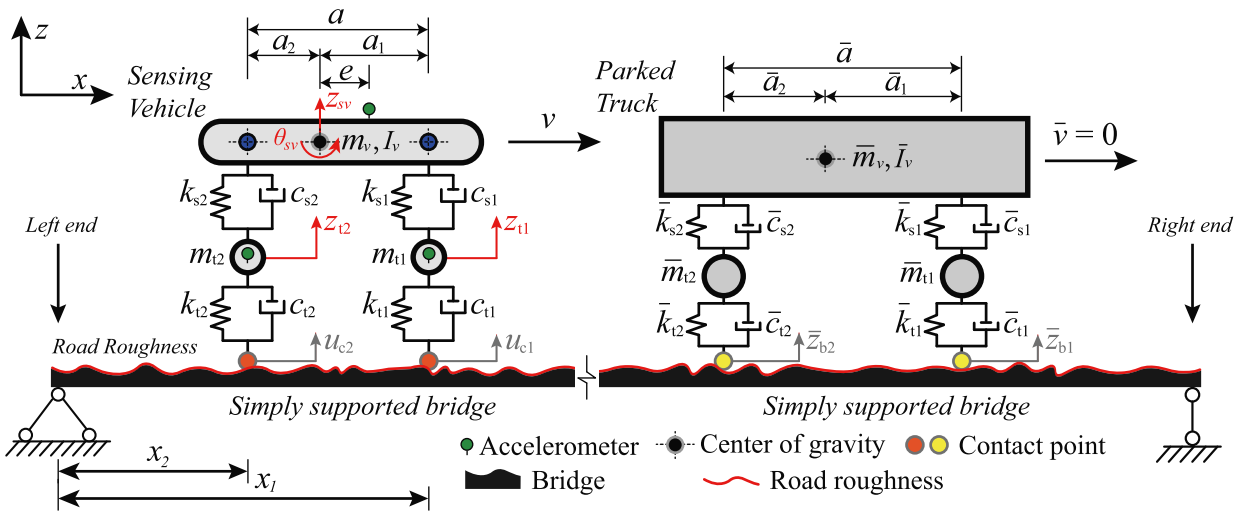

Fig. 1. VBI model.

external excitation input into the SV. In this paper, they are caused by unsmoothed road roughness and bridge vibrations through tires at the front and rear contact points. The displacements at contact points of the SV are represented by u_{c1} and u_{c2}, and the SV's input excitation can be calculated by Eq. (3).

$$\mathbf{z}_{sv} = [z_{sv}, \theta_{sv}, z_{t1}, z_{t2}]^T \tag{2}$$

$$\boldsymbol{f}_{cv} = [0, 0, k_{t1}u_{c1} + c_{t1}\dot{u}_{c1}, k_{t2}u_{c2} + c_{t2}\dot{u}_{c2}]^T \tag{3}$$

For the temporarily parked truck, a similar two-axle model is employed, and its properties are shown in Fig. 1. The truck is employed at different locations on the bridge to increase the amount of obtained modal information about the bridge and the sensitivity of its frequencies to local damage. Generally, a heavy truck's stiffness and damping values of wheels and suspensions are much higher than normal cars. It is found that when the stiffness is high enough, the truck's mass $M_{pt}^j = \overline{m}_v + \overline{m}_{t1} + \overline{m}_{t2}$ can be divided into two parts [46], as shown in Eq. (4),

$$\begin{aligned} M_{pt,1}^j &= \overline{m}_v \times \overline{a}_2/(\overline{a}_1 + \overline{a}_2) + \overline{m}_{t1} \\ M_{pt,2}^j &= \overline{m}_v \times \overline{a}_1/(\overline{a}_1 + \overline{a}_2) + \overline{m}_{t2} \end{aligned} \tag{4}$$

where $M_{pt,1}^j$ means the mass added to the position where the truck's front axle is on, and $M_{pt,2}^j$ is the mass added to the rear axle's position. j is utilized to present the position of the PT's rear axle on the bridge.

Bridge model. The bridge in this paper is simulated by a simply supported beam model. The total length of it is represented by L. It can be divided into N_n elements and N_s substructures. Each node has two DOFs: vertical translation and rotation in the X–Z plane. By excluding the two DOFs in the supports, the bridge has $2N_n$ DOFs in total. When the SV and other possible ongoing traffic cross the bridge, it will be stimulated by those vehicles. Under this condition, the bridge's vibration equilibrium equations can be represented by Eq. (5),

$$\mathbf{M}_b\ddot{\mathbf{z}}_b(t) + \mathbf{C}_b\dot{\mathbf{z}}_b(t) + \mathbf{K}_b\mathbf{z}_b(t) = \boldsymbol{f}_{b,N} \tag{5}$$

where $\mathbf{M}_b, \mathbf{C}_b$, and $\mathbf{K}_b$ are the mass, damping, and stiffness matrices of the simply supported bridge. $\ddot{\mathbf{z}}_b(t), \dot{\mathbf{z}}_b(t)$, and $\mathbf{z}_b(t)$ are the bridge's accelerations, velocities, and deflections at all DOFs. $\boldsymbol{f}_{b,N}$ are the forces applied to the bridge at all DOFs. Rayleigh viscous damping assumption is utilized to simulate the bridge's damping matrix, which is linearly combined by the mass and stiffness matrices and can be calculated by Eq. (6),

$$\mathbf{C}_b = \widetilde{\alpha}\mathbf{M}_b + \widetilde{\beta}\mathbf{K}_b \tag{6}$$

where $\widetilde{\alpha}$ and $\widetilde{\beta}$ can be obtained when two random damping ratios are determined in advance. Because it is always difficult to acquire detailed information regarding the relationship between the frequency and damping, typically, it is assumed that two identical damping ratios of the two control frequencies (e.g., first and second-order damping ratios [47]). Then, the coefficients $\widetilde{\alpha}$ and $\widetilde{\beta}$ can be calculated by Eq. (7),

$$[\widetilde{\alpha}, \widetilde{\beta}] = 2\xi/(f_{bm} + f_{bn})[f_{bm}f_{bn}, 1] \tag{7}$$

where ξ is the assumed damping ratio for the mth and nth order natural frequencies f_{bm} and f_{bn} of the bridge. After the coefficients $\widetilde{\alpha}$ and $\widetilde{\beta}$ are obtained, the bridge damping matrix $\mathbf{C}_b$ is calculated by Eq. (6). Eqs. (1) and (5) can be solved by Newmark-β approach by employing $\beta = 0.25$ and $\gamma = 0.5$ for unconditional stability.

Road roughness and interaction. The road roughness is simulated in accordance with ISO 8608 [48], which follows the power spectral density (PSD) function. The generation of road roughness can be performed using Eqs. (8) and (9),

$$G_d\left(n_{s,i}\right) = G_d\left(n_{s,0}\right)\left(\frac{n_{s,i}}{n_{s,0}}\right)^{-w} \tag{8}$$

$$z_r(x) = \sum_{i=1}^{N}\sqrt{2G_d\left(n_{s,i}\right)\Delta n_s}\cos\left(2\pi n_{s,i}x + \theta_i\right) \tag{9}$$

where $z_r(x)$ is the generated road roughness; x means the distance between the contact point and the bridge's left end (for example, x_1 and x_2 in Fig. 1); $n_{s,0}$ is the reference spatial frequency taken as 0.1 cycle/m, and $n_{s,i}$ represents the spatial frequency taken as numbers from 0.01 to 10 m^{-1}; Δn_s is the interval of spatial frequency that is selected as 0.01 cycle/m; θ_i means the random phase angle randomly sampled from a uniform distribution $p(\theta) = 1/2\pi, \theta \in [0, 2\pi]$; w is the fit exponent that is typically taken as 2; $G_d(n_{s,0})$ can be decided by the used class of road roughness. In this paper, A-class road roughness is employed; therefore $G_d(n_{s,0})$ can be specified as a random number ranging from 0 to 32×10^{-6} m^3 [49].

The interaction between the SV and bridge is accomplished by tires, road roughness, and the bridge's vibrations. When the SV is moving on the bridge, their interaction can be represented by Eqs. (10)–(14).

$$\boldsymbol{f}_{b,N} = \mathbf{N}_c\boldsymbol{f}_{cb} \tag{10}$$

$$\boldsymbol{f}_{cb} = \begin{bmatrix} k_{t1}\left(z_{t1} - u_{c1}\right) + c_{t1}\left(\dot{z}_{t1} - \dot{u}_{c1}\right) - m_v g \cdot a_2/(a_1 + a_2) - m_{t1}g \\ k_{t2}\left(z_{t2} - u_{c2}\right) + c_{t2}\left(\dot{z}_{t2} - \dot{u}_{c2}\right) - m_v g \cdot a_1/(a_1 + a_2) - m_{t2}g \end{bmatrix} \tag{11}$$

$$\mathbf{N}_c = \begin{bmatrix} 0 & \cdots & 0 & \cdots & \chi_1 & \cdots & 0 \\ 0 & \cdots & \chi_2 & \cdots & 0 & \cdots & 0 \end{bmatrix}^T_{2\times 2N_n} \tag{12}$$

$$\chi_i = \left[1 - 3d_i^2 + 2d_i^3, d_i l_e \left(d_i - 1\right)^2, 3d_i^2 - 2d_i^3, d_i l_e \left(d_i^2 - d_i\right)\right]_{1\times 4}, i = 1, 2. \tag{13}$$

$$d_i = (x_i(t) - (q-1)l_e)/l_e, i = 1, 2. \tag{14}$$

Here, assuming that the ith wheel of the SV is on the qth finite element of the bridge (counted from the left end), $x_i(t)$ represents the distance between the ith wheel and the bridge's left end, as shown in Fig. 1. χ_i represents the force distribution coefficients for the ith wheel. Then, χ_i is put into the matrix $\mathbf{N}_c$ for distributing the contact force between the vehicle and the bridge. It is noted that only the bridge's DOFs that can receive the distributed force are non-zero, and other entries in the matrix $\mathbf{N}_c$ are zeros. l_e means the length of the bridge's elements. The contact-point forces applied to the bridge is denoted by $\boldsymbol{f}_{cb}$, in which the subscript c represents the contact point and b means the bridge. Then, the contact-point deflections and velocities of the bridge can be calculated by Eq. (15). The displacement and velocity at the ith contact point can be calculated by $u_{ci} = z_{cbi} + z_{ri}, i = 1, 2.$, where z_{ri} is the road roughness calculated by Eq. (9) at the ith contact point; $(')$ means the derivatives to x. The collected responses at contact points will be utilized in Eqs. (1)–(3) to calculate the vehicular responses. After a number of iterations utilizing the aforementioned equations, the bridge's deflection difference between two iterations will converge at a predetermined tolerance.

$$\begin{cases} \mathbf{z}_{cb} = \left[z_{cb1}, z_{cb2}\right]^T = \mathbf{N}_c^T \mathbf{z}_b \\ \dot{\mathbf{z}}_{cb} = \left[\dot{z}_{cb1}, \dot{z}_{cb2}\right]^T = v\left(\mathbf{N}_c'\right)^T \mathbf{z}_b + \mathbf{N}_c^T \dot{\mathbf{z}}_b \end{cases} \tag{15}$$

2.1.2. Back-calculated CP responses

As aforementioned, it has been demonstrated that the CP response is preferable than vehicle accelerations for inferring the modal characteristics of a bridge. One advantage of using the CP response is that it does not include the vehicle's information, and it only consists of two sources: road roughness and bridge vibrations. However, few studies have explored deriving the vehicle's CP responses when the damping of tires and suspensions is considered simultaneously. This section will discuss back-calculating the CP response of a half-car (HC) model and further reducing the influence of road roughness by using the residual CP response of two wheels.

By disassembling Eq. (1) and selecting dynamic equilibrium equations of wheels, we can get Eqs. (16) and (17),

$$m_{t1}\ddot{z}_{t1} - c_{s1}(\dot{z}_{sv} - \dot{z}_{t1} + a_1\dot{\theta}_{sv}) - k_{s1}\left(z_{sv} - z_{t1} + a_1\theta_{sv}\right) + c_{t1}\left(\dot{z}_{t1} - \dot{u}_{c1}\right) + k_{t1}\left(z_{t1} - u_{c1}\right) = 0 \tag{16}$$

$$m_{t2}\ddot{z}_{t2} - c_{s2}(\dot{z}_{sv} - \dot{z}_{t2} - a_2\dot{\theta}_{sv}) - k_{s2}\left(z_{sv} - z_{t2} - a_2\theta_{sv}\right) + c_{t2}\left(\dot{z}_{t2} - \dot{u}_{c2}\right) + k_{t2}\left(z_{t2} - u_{c2}\right) = 0 \tag{17}$$

where u_{c1} and u_{c2} are the CP response of the front and rear wheels. By taking the second-order derivative of the above two equations and putting items related to CP responses to the left side, we can obtain Eqs. (18)–(20).

$$\ddot{u}_{ci} + \frac{c_{ti}}{k_{ti}}\frac{d\ddot{u}_{ci}}{dt} = \Psi_i(t), i = 1, 2. \tag{18}$$

$$\Psi_1(t) = \frac{m_{t1}}{k_{t1}}\frac{d^2\ddot{z}_{t1}}{dt^2} - \frac{c_{s1}}{k_{t1}}\left(\frac{d\ddot{z}_{sv}}{dt} - \frac{d\ddot{z}_{t1}}{dt} + a_1\frac{d\ddot{\theta}_{sv}}{dt}\right) - \frac{k_{s1}}{k_{t1}}\left(\ddot{z}_{sv} - \ddot{z}_{t1} + a_1\ddot{\theta}_{sv}\right) + \ddot{z}_{t1} + \frac{c_{t1}}{k_{t1}}\frac{d\ddot{z}_{t1}}{dt} \tag{19}$$

$$\Psi_2(t) = \frac{m_{t2}}{k_{t2}}\frac{d^2\ddot{z}_{t2}}{dt^2} - \frac{c_{s2}}{k_{t2}}\left(\frac{d\ddot{z}_{sv}}{dt} - \frac{d\ddot{z}_{t2}}{dt} - a_2\frac{d\ddot{\theta}_{sv}}{dt}\right) - \frac{k_{s2}}{k_{t2}}\left(\ddot{z}_{sv} - \ddot{z}_{t2} - a_2\ddot{\theta}_{sv}\right) + \ddot{z}_{t2} + \frac{c_{t2}}{k_{t2}}\frac{d\ddot{z}_{t2}}{dt} \tag{20}$$

Here, k_{ti}, c_{ti}, k_{si} and c_{si} can be measured by experiments, and the accelerations of the wheels can be recorded [50]. However, installing SV's body sensor precisely in the center of gravity is rather difficult. In Fig. 1, we assume that there is an error e when installing the body sensor. Thus, the vertical and angular accelerations collected by the body sensor can be obtained using Eq. (21)a. Accordingly, the SV's body sensor position need to be updated as represented by Eq. (21)b.

$$\ddot{\hat{z}}_{sv} = \ddot{z}_{sv} + e\ddot{\theta}_{sv}; \ddot{\hat{\theta}}_{sv} = \ddot{\theta}_{sv} \tag{21a}$$

$$\hat{a}_1 = a_1 - e; \hat{a}_2 = a_2 + e \tag{21b}$$

Then, by substitute $\ddot{z}_{sv}, \ddot{\theta}_{sv}, a_1$ and a_2 by $\ddot{\hat{z}}_{sv}, \ddot{\hat{\theta}}_{sv}, \hat{a}_1$ and $\hat{a}_2$, the error e can be eliminated automatically. This means that the proposed method does not need the center of gravity to be located precisely but merely requires the distances between axles and the body sensor to be measured. It is also worth noting that the above deduction is based on the assumption that the vehicle's body is rigid, despite that the fact that small deformations are common in practical engineering. Therefore, the SV's body sensor is suggested to be as close to the center of gravity as possible.

In Eqs. (19) and (20), since we only collect the SV's accelerations, their first-order and second-order differentials to time t need to be approximately calculated by Eq. (22),

$$\frac{dZ}{dt} = \frac{Z(s) - Z(s-1)}{\Delta t}, \frac{d^2Z}{dt^2} = \frac{Z(s+1) - 2Z(s) + Z(s-1)}{(\Delta t)^2} \tag{22}$$

where s means the sth sampling point. Δt is the sampling time interval, and it can be obtained by $\Delta t = 1/f_s$ where f_s is the sampling frequency. Consequently, by approximate computations, we can get $\Psi_1(t)$ and $\Psi_2(t)$. As Eq. (18) is a first-order linear differential equation, its solution can be represented by Eq. (23) when the accelerations are collected in the discrete format in practical engineering.

$$\ddot{u}_{ci}(t) = \begin{cases} \Psi_i(t), i = 1, 2. \quad \text{if } c_{ti} = 0 \\ \eta_i\left(\sum_{s=1}^{t/\Delta t} \Psi_i|_s \exp\left(\eta_i(s\Delta t - t)\right)\Delta t\right), i = 1, 2; s = 1, 2, \ldots \text{ if } c_{ti} \neq 0 \end{cases} \tag{23}$$

Here, $\eta_i = k_{ti}/c_{ti}, i = 1, 2$ is defined as the ratio of the stiffness and damping of the SV's tires. Δt is the same as Eq. (22); s represents the sth sampling point of the SV's accelerations. Therefore, by employing Eq. (23), the SV's CP responses of front and rear wheels can be obtained. However, as the CP responses $\ddot{u}_{ci} = \ddot{z}_{cbi} + \ddot{z}_{ri}, i = 1, 2$, the scale of road roughness is much greater than that of the bridge's vibrations. Thus, the calculated CP response is mainly related to the road roughness rather than the bridge. To tackle the above problem, after the CP responses of the front and rear axles are obtained, the rear axle's CP response will be subtracted from the front axle's CP response with a time lag Δt_g to obtain the residual CP response, which can help with eliminating the influence of road roughness. The time lag can be calculated by $\Delta t_g = (a_1 + a_2)/v$. For vehicles, the stiffness-damping ratio is generally the same for front and rear tires, meaning that $\eta = \eta_1 = \eta_2$. Therefore, the process of calculating the residual CP response can be represented by Eq. (24). Further, the fast Fourier transformation (FFT) will be employed to transform the time-domain residual CP response into the frequency domain, and the bridge's frequencies can be identified manually. In the subsequent sections, for simplicity, the residual CP responses are represented by $\ddot{u}_{c1} - \ddot{u}_{c2}$, and the function arguments are omitted for clarity.

$$\ddot{u}_{c1}(t) - \ddot{u}_{c2}(t + \Delta t_g) = \begin{cases} \Psi_1(t) - \Psi_2(t + \Delta t_g) \quad \text{if } c_{ti} = 0 \\ \eta\Delta t\left(\sum_{s=1}^{t/\Delta t} \Psi_1|_s \exp\left(\eta(s\Delta t - t)\right) - \Psi_2|_{s+\frac{\Delta t_g}{\Delta t}} \exp(\eta((s + \frac{\Delta t_g}{\Delta t})\Delta t - t))\right) \\ s = 1, 2, \ldots \text{ if } c_{ti} \neq 0 \end{cases} \tag{24}$$

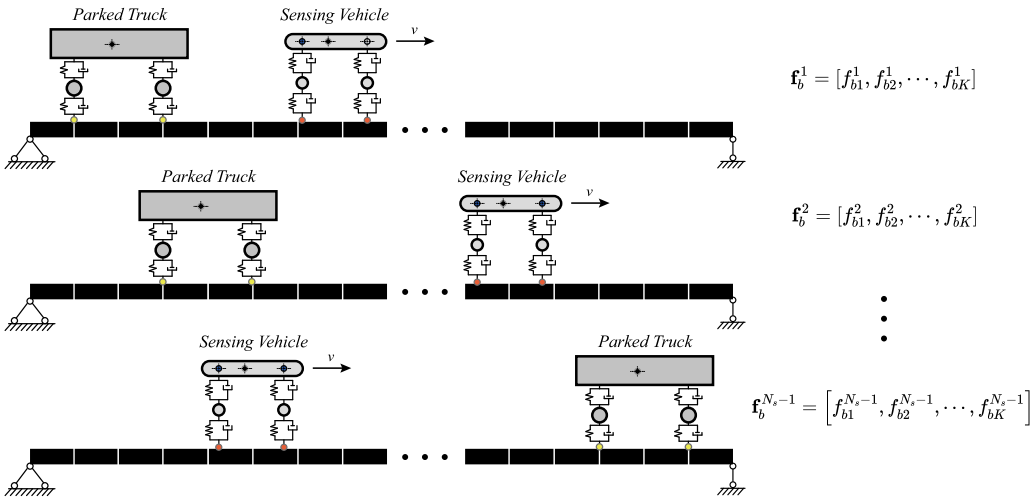

Fig. 2. Illustration of the bridge with SV and PT at different locations.

2.2. Damage detection

In this section, the damage detection strategy utilizing the indirectly identified bridge frequencies will be introduced. The proposed method includes an SV employed to indirectly identify the bridge's natural frequencies and a PT parked at different positions on the bridge to increase the amounts of modes and the bridge's sensitivity to local damage. When the PT is parked at a specific location, the SV is used to identify the bridge's natural frequencies once. Two objective functions using the identified frequencies are utilized to detect the bridge's damage.

2.2.1. Damage simulation

The bridge's damage is simulated by stiffness reduction, and it is represented by damage factors $\boldsymbol{\mu} = [\mu_1, \mu_2, \ldots, \mu_{N_s}]$, where μ_j means the ratio of stiffness after the jth substructure is damaged to the original stiffness. For example, $\mu_2 = 0.8$ means that the second substructure's stiffness is reduced by 20%. If $\mathbf{K}_j$ is utilized to symbolize the extended stiffness matrix of the jth substructure in the global coordinate, the stiffness matrix of the damaged (possible) bridge becomes Eq. (25).

$$\mathbf{K}_b^d(\boldsymbol{\mu}) = \sum_{j=1}^{N_s} \mu_j \mathbf{K}_j \tag{25}$$

2.2.2. Temporarily parked truck

(1) Frequency vector formation when the PT is at different locations

The employed PT is supposed to be heavy enough to change the bridge's natural frequencies (as an alternation of the bridge's mass). When it is parked on $N_s - 1$ different locations (substructures) of the bridge, the bridge's natural frequencies (with the PT) will change accordingly. When the PT's rear axle is on the jth location, the bridge's first K order frequencies can be indirectly identified by the SV as $\mathbf{f}_b^j = [f_{b1}^j, f_{b2}^j, \ldots, f_{bK}^j]^T$, which is illustrated in Fig. 2. Thus, we can get $(N_s - 1) \times K$ frequency information of the bridge by introducing the PT. All identified frequencies can be combined together to form a frequency vector, as shown in Eq. (26).

$$\mathbf{f}_b = [\mathbf{f}_b^1, \mathbf{f}_b^2, \ldots, \mathbf{f}_b^{N_s-1}]^T \tag{26}$$

(2) Determination of the truck's mass

In addition to increasing the amounts of used modes, the PT is intended to raise the sensitivity of the bridge's natural frequencies to local damage. The relative sensitivity of the kth natural frequency with respect to the damage factor of the lth substructure when the mass $(M_{pt,i}^j, i = 1, 2.)$ is on the jth location can be calculated by Eq. (27),

$$R_{kjl}(\boldsymbol{\mu}, M_{pt,i}^j) = \frac{\partial f_{b,kj}(\boldsymbol{\mu}, M_{pt,i}^j)}{\partial \mu_l} = \frac{\psi_{b,kj}^T(\boldsymbol{\mu}, M_{pt,i}^j)\mathbf{K}_l\psi_{b,kj}(\boldsymbol{\mu}, M_{pt,i}^j)}{2f_{b,kj}(\boldsymbol{\mu}, M_{pt,i}^j)} \tag{27}$$

where $\psi_{b,kj}$ is the modal shape vector; $\mathbf{K}_l$ denotes the extended stiffness matrix of the lth substructure. In practice, $M_{pt,i}^j$ can vary at various locations to increase the relative sensitivity of different substructures, but it is difficult to change the mass of the PT during the assessment. Thus, the mass is assumed as the same value in this study. Therefore, the proposed method merely requires moving the PT along the bridge to different locations. By employing Eq. (27), the sensitivity of mass to each substructure for the undamaged bridge can be obtained to determine the proper mass of the PT.

2.2.3. Objective functions

The proposed method is model-based and requires the bridge's FE model. After the PT is parked at a particular location, the bridge's mass matrix needs to be altered to include the effects of the PT. Assume that $\mathbf{M}_{b,j}$ is utilized to represent the bridge's mass matrix when the PT's rear axle is on the jth location. We can obtain the bridge FE model's frequency vector $\mathbf{f}_b(\boldsymbol{\mu})$ using the eigenvalue decomposition of the structural stiffness and mass matrices $\mathbf{K}_b^d(\boldsymbol{\mu})$ and $\mathbf{M}_{b,j}$. Eq. (28) demonstrates a conventional method for minimizing the relative error between the frequencies of the FE model and the experimental bridge (objective function L_1), in which $\|\cdot\|$ represents the Euclidean norm. The L_1 function has been utilized in several existing studies [38,51,52].

$$L_1(\boldsymbol{\mu}) = \|(\mathbf{f}_b(\boldsymbol{\mu}) - \mathbf{f}_b)/\mathbf{f}_b\|_2^2 \tag{28}$$

In this paper, we proposed a new objective function L_2 that integrates the MAC values between the frequency vectors, as shown in Eqs. (29) and (30).

$$L_2(\boldsymbol{\mu}) = 1 - \mathrm{MAC}(\mathbf{f}_b(\boldsymbol{\mu}), \mathbf{f}_b) + \lambda\|1 - \boldsymbol{\mu}\|_1 \tag{29}$$

$$\mathrm{MAC}(\mathbf{f}_b(\boldsymbol{\mu}), \mathbf{f}_b) = \frac{|\mathbf{f}_b^T(\boldsymbol{\mu})\mathbf{f}_b|^2}{(\mathbf{f}_b^T(\boldsymbol{\mu})\mathbf{f}_b(\boldsymbol{\mu}))(\mathbf{f}_b^T\mathbf{f}_b)} \tag{30}$$

where the term $\lambda\|1-\boldsymbol{\mu}\|_1$ means the l_1-norm of $1-\boldsymbol{\mu}$, which can promote the sparsity of the identified damage, and it is beneficial to locate the position of possible damage in the bridge [32,53,54].

Table 1
Parameters of the SV.

Parameter	Symbol	Value
Body mass	m_v	542.5 kg
Body moment of inertia	I_v	550.0 kg·m^2
Wheel mass	m_{t1}, m_{t2}	40.0 kg
Suspension stiffness	k_{s1}, k_{s2}	10000, 10000 N/m
Suspension damping	c_{s1}, c_{s2}	2000, 2000 N·s/m
Tire stiffness	k_{t1}, k_{t2}	150000, 150000 N/m
Tire damping	c_{t1}, c_{t2}	430, 430 N·s/m
Constants	a_1, a_2	1.4, 1.47 m
Speed	v	5.0 m/s
Frequencies	$f_{sv1}, f_{sv2}, f_{sv3}, f_{sv4}$	0.9348, 1.3335, 10.0699, 10.0718 Hz

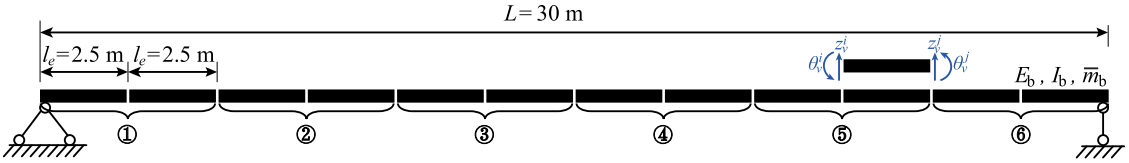

Fig. 3. FE model of the bridge.

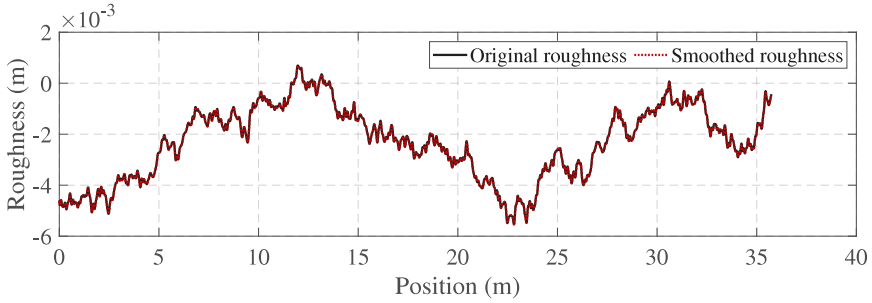

Fig. 4. Generated road roughness.

3. Simulations and case study

3.1. Parameters of the VBI system

The parameters of the employed SV are illustrated in Table 1, which is adopted from the Ref. [55]. The damping values of suspensions and tires are referred to the sensing vehicle in Ref. [56]. To verify the effectiveness of identifying the bridge's frequencies using residual CP responses of the SV, the PT is temporarily not considered in Sections 3.1 and 3.2.

The parameters of the bridge are referred to the Ref. [57], in which its length is $L = 30$ m, the mass of unit length is $\overline{m}_b = 6000$ kg/m, and the bending stiffness is $E_b I_b = 2.5 \times 10^{10}$ N/m^2. The bridge's FE model is shown in Fig. 3. There are six substructures, and each one has two finite elements. Utilizing the FE model of the undamaged bridge (namely $\boldsymbol{\mu} = [1, 1, 1, 1, 1, 1]$) without PT, we can get its first three natural frequencies: $f_{b1} = 3.5627$ Hz, $f_{b2} = 14.2513$ Hz, and $f_{b3} = 32.0721$ Hz. Also, it can be noticed that the mass ratio of the SV and the bridge is $(542.5 + 40 + 40)/6000/30 = 0.35\%$. When it passes the bridge, such a little mass will not induce a change in the bridge's frequencies.

The road roughness is generated by Eqs. (8) and (9) with $G_d(n_{s,0}) = 4 \times 10^{-6}$ m^3. However, according to studies conducted by Yang et al. [30], the vehicle will not be affected by point-wise road roughness when crossing the bridge. Rather, it is an area where the vehicle's tire and the bridge are contacted with each other. In this study, a moving average function is utilized to smooth the generated road roughness. Fig. 4 shows the original and smoothed road roughness. The generated road roughness length is 35.47 m.

3.2. Indirect bridge frequency identification using CP responses

This section introduces two cases: purely smooth and A-class road roughness without PT, to verify the proposed method to identify the bridge's frequencies using the SV. The bridge's damping is temporarily ignored and will be detailedly discussed in Section 4.3.

(1) Purely smooth roughness

When the road roughness is purely smooth, the SV's accelerations are shown in Fig. 5a. It can be seen that the scale of the wheels' vibrations is greater than the SV's body vibrations, and all signals are in $[-2, 2] \times 10^{-3}$ m/s^2. By transforming the acceleration signals into the frequency domain using FFT, Fig. 5b is obtained. We can see that even though only the accelerations are utilized, the bridge's frequencies can be identified with the second and third frequencies divided into two distinct frequencies (called camel hump phenomenon [58]). The separated frequencies are $f_{bn}^l = f_{bn} - n\pi v/L$ and $f_{bn}^r = f_{bn} + n\pi v/L$ [59]. Thus, when the objective is to identify the bridge's frequency, we need to calculate its higher order frequencies by $f_{bn} = (f_{bn}^l + f_{bn}^r)/2$. From this case, we can conclude that the bridge's dynamic information is contained in the SV's vibrations. However, in practical engineering, road roughness is generally complex rather than purely smooth; advanced approaches must be considered to remove the influence of road roughness.

(2) A-class road roughness

This section will employ the smoothed road roughness presented in Fig. 4. The SV's accelerations in the time and frequency domain are shown in Fig. 6. It can be seen that the scale of the SV's accelerations increases significantly due to the effects of road roughness, but the bridge's frequencies are no longer visible in the frequency domain. High peaks are primarily located around f_{sv3} and f_{sv4}. Thus, the inverse influence of road roughness needs to be addressed properly.

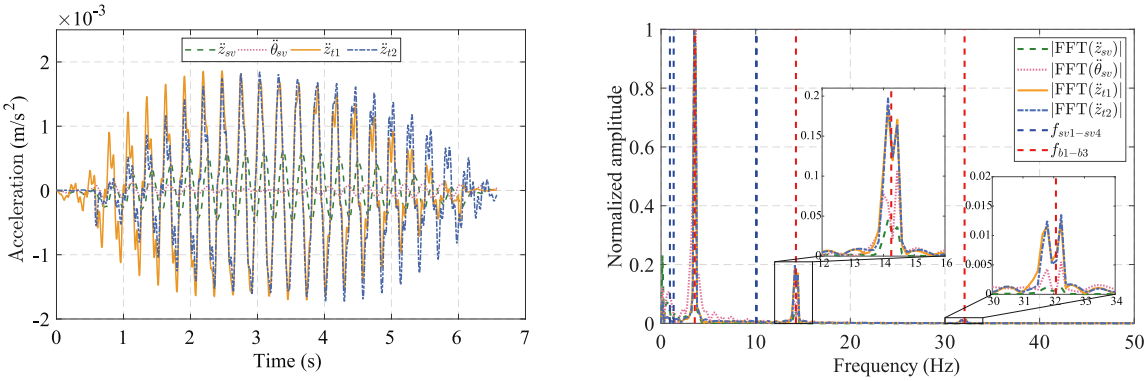

(a) SV's accelerations (b) SV's frequency spectrum (normalized)

Fig. 5. SV's time- and frequency-domain responses with smooth roughness.

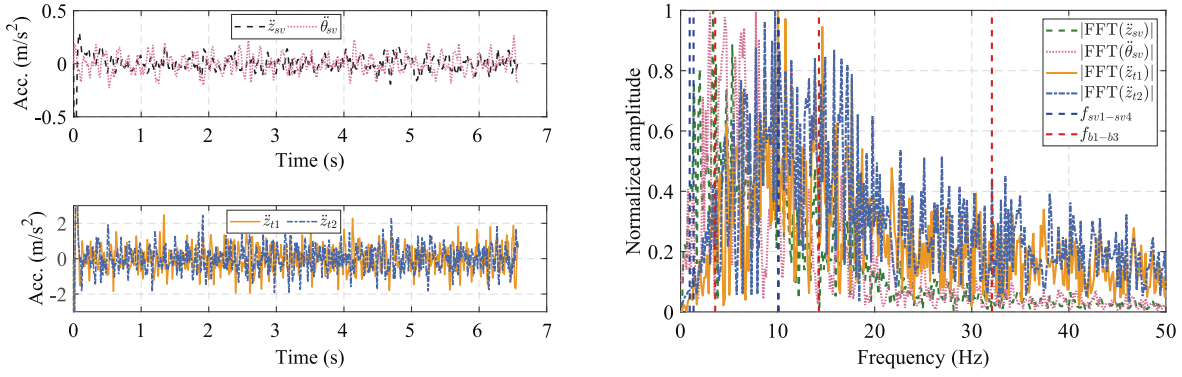

(a) SV's accelerations (b) SV's frequency spectrum (normalized)

Fig. 6. SV's time- and frequency-domain responses with A-class roughness.

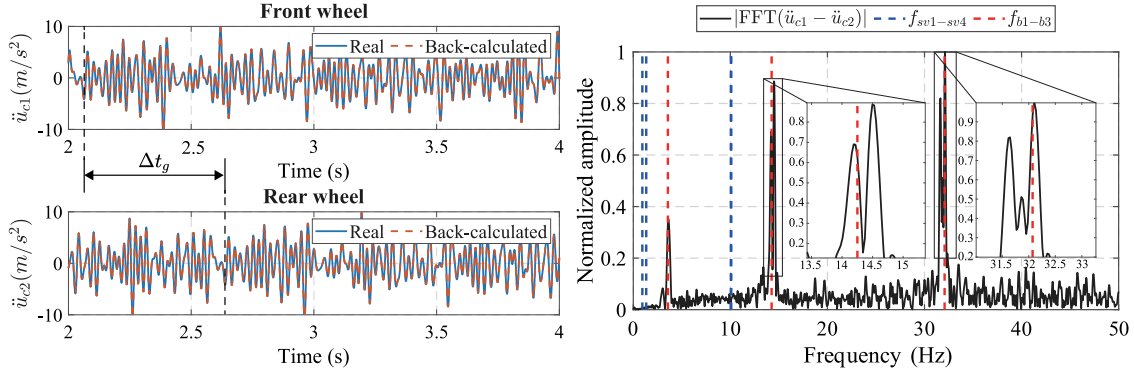

(a) CP response of the front and rear wheels (b) Residual CP frequency spectrum

Fig. 7. Indirect bridge frequency identification using residual CP responses.

In the simulations, real CP responses are known (but generally unknown in practical engineering). Fig. 7a shows CP responses calculated by Eq. (23). We can see that the obtained CP responses are in good precision, which verifies the proposed method to back-calculate the CP response from the SV's accelerations. Further, it is clear that the rear wheel's CP response delay with a time lag of Δt_g compared to that of the front wheel. It shows that the influence of road roughness plays a main role in the time-domain CP responses. By subtracting the rear wheel's CP responses from the front wheel's CP responses using Eq. (24) and transforming the residual time-domain signals into the frequency domain, Fig. 7b is obtained.

It is clear that the bridge's frequencies are outstanding in the frequency domain when the residual CP response is employed. The SV's frequencies and influence of road roughness are mostly eliminated. However, we can also see that the identified bridge frequencies diverge from the ground truth, especially when the camel hump phenomenon occurs in higher modes. As a result, it is hard to solely utilize the indirectly identified frequencies for the damage detection purpose as we do not know whether the error between the identified and true frequency is caused by the indirect identification method or the damage. In other words, the indirectly identified modal information is limited for damage detection. Hence, to decrease the influence of

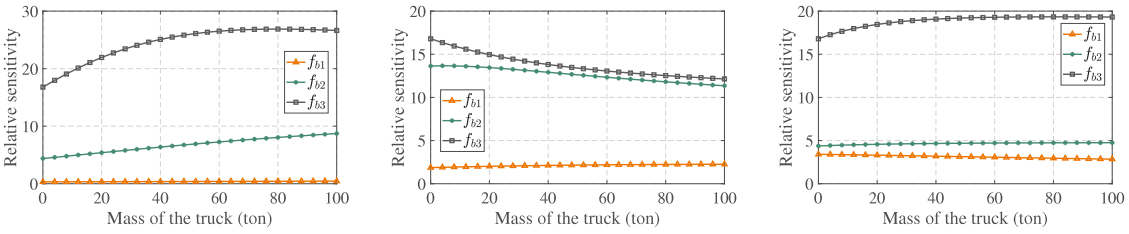

(a) Substructure 1/6 (b) Substructure 2/5 (c) Substructure 3/4

Fig. 8. Relative sensitivity with respect to mass on substructures.

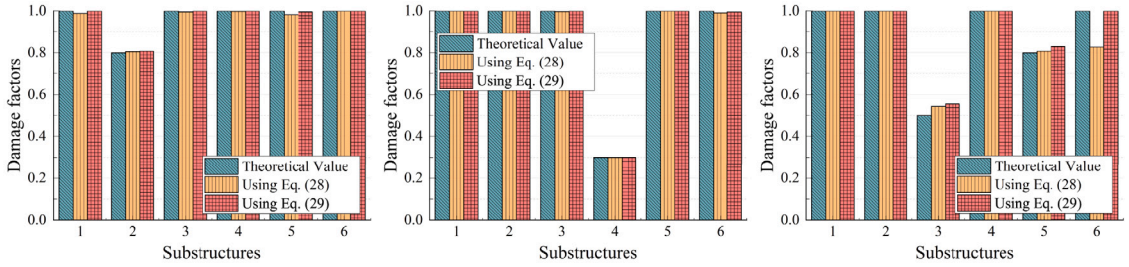

(a) Scenario 1 (b) Scenario 2 (c) Scenario 3

Fig. 9. Damage detection results for different scenarios: case study.

frequency identification error, the PT is introduced to boost the modal information about the bridge for further damage detection.

3.3. Damage detection using identified frequencies

3.3.1. Determination of the truck's mass

The initial step in employing a PT is determining its mass value M_{pt}^{j}. The PT is introduced to increase the amounts of modes and the bridge's sensitivity to local damage. In this paper, the PT's mass is determined via sensitivity analysis. The relative sensitivity with respect to the mass $M_{pt,i}^{j}$ when it is on different substructures is plotted in Fig. 8. As the simply supported bridge is symmetric, the relative sensitivity values of the first and sixth substructures are the same, and so are other symmetric substructures.

For substructure 1, it can be seen that f_{b1} is not quite sensitive (around zero) to the PT's mass, but with the increase in the mass value, the sensitivity of f_{b2} and f_{b3} rises. When the mass climbs roughly to 60 tons, the sensitivity of f_{b3} approaches the peak. Therefore, for the first substructure, the mass of 60 tons is proper. However, for the second substructure, we can notice that, similarly, the sensitivity of f_{b1} does not change much with the growth of the PT's mass. But the sensitivity of f_{b2} and f_{b3} decrease when the mass value increases, especially when the mass exceeds 15 tons for f_{b2}. Thus, to preserve the higher sensitivity of the second substructure, the mass value is supposed to be fewer than 15 tons. For the third substructure, it can be noticed that f_{b1} and f_{b2} are not affected by an increase in the PT's mass value. For f_{b3}, even if there is an increase in sensitivity, the increment is not huge. In addition to considering the PT's mass, the allowed weight of trucks on the bridge should also be considered. In this paper, a 25-ton truck is employed with the following parameters: $\overline{a}_1 = 2.6$ m, $\overline{a}_2 = 2.4$ m, $\overline{m}_{t1} = 1000$ kg, $\overline{m}_{t2} = 1500$ kg. For the PT's mass, the authors would recommend around 10% of the bridge's total mass, which can induce the change of the bridge's frequencies and also is generally allowable for short-span bridges.

3.3.2. Damage detection

This section examines three damage scenarios, including single minor damage, single large damage, and multiple damages. Additionally, the damage occurs in different locations. All damage scenarios are listed below:

Table 2
Identified frequencies of the case study (Hz)

PT's position		$j = 1$	$j = 2$	$j = 3$	$j = 4$	$j = 5$
Scenario 1	f_{b1}^{j}	3.4485	3.2959	3.1738	3.1738	3.3264
	f_{b2}^{j}	13.3667	12.5122	13.4888	13.3972	12.5427
	f_{b3}^{j}	29.9377	30.1819	29.9683	30.0903	30.0903
Scenario 2	f_{b1}^{j}	2.7466	2.6245	2.4719	2.4414	2.4719
	f_{b2}^{j}	12.8174	11.8713	12.7869	12.8479	12.2070
	f_{b3}^{j}	27.4963	27.5269	27.6489	27.0386	27.0386
Scenario 3	f_{b1}^{j}	3.0823	2.9907	2.7771	2.8076	3.0212
	f_{b2}^{j}	12.8174	11.8713	12.7563	12.8174	11.7188
	f_{b3}^{j}	27.8320	27.9236	28.1677	28.3203	28.5034

Scenario 1: single minor damage, $\boldsymbol{\mu} = [1, 0.8, 1, 1, 1, 1]$;
Scenario 2: single large damage, $\boldsymbol{\mu} = [1, 1, 1, 0.3, 1, 1]$;
Scenario 3: multiple damages, $\boldsymbol{\mu} = [1, 1, 0.5, 1, 0.8, 1]$.

For scenarios 1 and 2, the damage occurs only in one location, namely substructure 2 with a 20% stiffness reduction and substructure 4 with a 70% stiffness reduction. For scenario 3, there are two damaged locations: substructure 3 with a 50% stiffness reduction and substructure 5 with a 20% stiffness reduction. All other parameters are the same as Section 3.2. The PT is employed to park at different locations. For various scenarios, when the PT's rear axle is parked on positions from 1 to 5, the indirect frequency identification results are provided in Table 2.

It can be noticed that after the PT is parked on the bridge, the bridge's natural frequencies decrease. Additionally, when it is on different locations, the decrease degrees of f_{b1}, f_{b2} and f_{b3} are not the same. These modal parameters with external mass can provide more information about the bridge's damage. Employing Eqs. (28) and (29), the optimized damage factors $\boldsymbol{\mu}$ are shown in Fig. 9.

It can be seen from Fig. 9 that even though there are inaccuracies when indirectly identifying the bridge's frequencies using SV's accelerations, the bridge's damage can be detected accurately when the PT is introduced. Also, we can see that damage detection is more accurate when there is a single damage instead of multiple damages. When the traditional objective function utilizing the relative errors is employed, some substructures are prone to be wrongly identified as damaged, e.g., substructures 6 in scenario 3. The above problem can

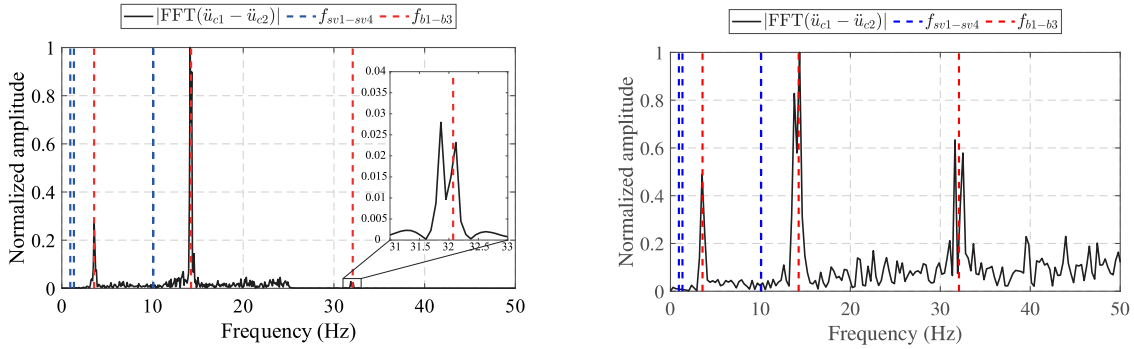

(a) Speed of 2.5 m/s (b) Speed of 8.3 m/s

Fig. 10. Indirect bridge frequency identification with different speeds.

be overcome by the proposed novel objective function. The erroneous detection results are rectified.

4. Investigation on influence factors

In Section 3, a case study is investigated, and it shows promising results of damage detection. In this section, other influence factors, including the speed of the SV, environmental noise, and bridge damping, will be discussed. Further, the proposed method is employed in a more practical case to verify its effectiveness. The parameters utilized are the same as the ones in Section 3.3 unless there are special statements.

4.1. Sensing vehicle speed

The speed of the SV can significantly influence the precision of indirect bridge frequency identification. One reason is that in the VBI system, the vehicle plays two roles: the exciter and the signal collector. If the SV moves slowly, the bridge may not be sufficiently stimulated, and then its dynamic information cannot be transferred to the vehicle, particularly for the higher modes. However, if the SV's speed is high, the bridge may vibrate significantly but the passage time will be shortened greatly. After using FFT to transform the short-time signals into the frequency domain, the frequency resolution will be pretty poor, making the frequency identification results less accurate, and further poor accuracy of damage detection. In this study, we employed two kinds of speeds 2.5 m/s (9 km/h) and 8.3 m/s (30 km/h). The frequency identification results using the SV's residual CP response are shown in Fig. 10.

It can be seen that when the speed is low (say 2.5 m/s), the frequency resolution is fine, which is conducive to accurately identifying the bridge frequency. However, we can notice that the bridge's third frequency is quite weak. When the speed changes to 8.3 m/s, we can see that the bridge's first three frequencies are highlighted in the frequency domain. In addition, it is seen that due to the increase in speed, the frequency resolution becomes poorer compared to Fig. 7b. The identified frequency values (with PT at different positions) when the SV's speed is 2.5 and 8.3 m/s can be found in Table A1 in Appendix B. Figs. 11 and 12 have plotted the damage detection results using identified frequency values by the SV.

From Fig. 11, we can see that when the speed is relatively low, the damage detection results are still accurate for all scenarios. When the new objective functions (Eq. (29)) are employed, the wrongly identified damaged substructures by Eq. (28) are corrected (see substructure 6 in scenario 3). When the SV's speed increases to 8.3 m/s, as shown in Fig. 12, we can see that due to the poor frequency resolution, the damage detection results become worse. For scenarios 1 and 3, Eq. (28) has identified the damage positions by mistake. By employing the MAC-based objective function, the damaged substructures and degrees are successfully identified. Therefore, we can conclude that (1) the increase in speed will decrease the frequency resolution, making poor identification of the bridge's frequencies using the SV, which inversely influences damage detection, and (2) the proposed MAC-based objective function can improve the robustness of damage detection when different SV speeds are employed.

Table 3
Ongoing traffic.

Ongoing traffic	SV	V1	V2	V3	V4
Entry time (s)	0	0.860	−4.214	1.980	−3.004

4.2. Noise level

It is unavoidable to incorporate environmental noises when collecting the vehicle's vibration data. This section considers different ambient noises for bridge damage detection using the indirectly identified frequencies. The noises are added to the original acceleration signals by Eq. (31),

$$\ddot{z}_v^p = \ddot{z}_v + E_p N_s \sigma_{\ddot{z}_v} \tag{31}$$

where $\ddot{z}_v^p$ is the polluted vehicle accelerations; $\ddot{z}_v$ is the vehicle's original vibrations without noises, and it represents $\ddot{z}_{sv}, \ddot{\theta}_{sv}, \ddot{z}_{t1}$ or $\ddot{z}_{t2}$; E_p means the noise level; N_s means numbers sampled from the standard normal distribution; $\sigma_{\ddot{z}_v}$ is the standard deviation of the acceleration $\ddot{z}_v$. The SV's all accelerations will be polluted by the environmental noises, and then the contaminated signals are input into Eq. (24) to calculate the residual CP responses. Fig. 13a shows the polluted accelerations of the SV's rear wheel. After the accelerations, including 1% environmental noises, are utilized for calculating the residual CP responses, the indirect frequency identification results are shown in Fig. 13b. It can be seen that the bridge's first two frequencies are identifiable but rather faint in the frequency domain. The third bridge frequency has been totally overshadowed by ambient noises. This is because the environmental noises are randomly collected by the sensors, and they cannot be eliminated by subtracting the rear wheel's signals from the front wheel's accelerations.

In the above analysis, the ongoing traffic is not included, yet it is unavoidable in practical engineering. Indeed, one advantage of the indirect frequency identification method is that it does not need to interrupt the ongoing traffic. In this paper, four ongoing additional vehicles (V1–V4) with the same parameter of the SV are considered. But it is worth noting that the ongoing traffic can have different vehicle parameters and speeds [7]. It is assumed that the SV enters the bridge at 0 s. All vehicles' entering time and speed are listed in Table 3.

Fig. 14 has plotted the indirect frequency identification results when V1 and V2 are considered as the ongoing traffic under 1% and 3% noise levels. The comparison between Figs. 13b and 14a shows the "positive" influence of the ongoing traffic, which can partially weaken the inverse

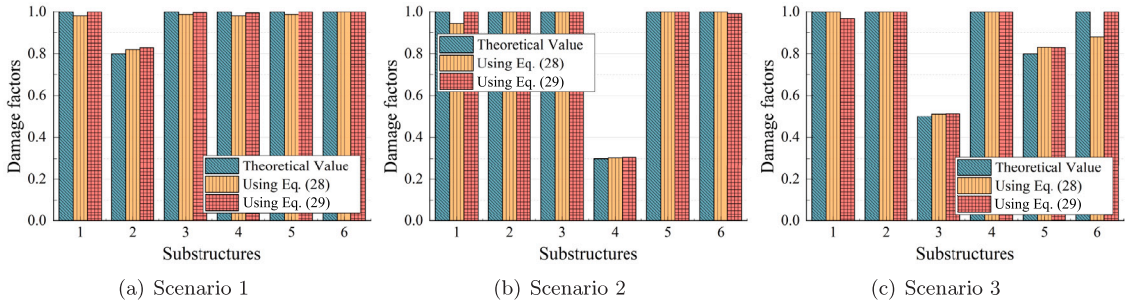

(a) Scenario 1 (b) Scenario 2 (c) Scenario 3

Fig. 11. Damage detection results for different scenarios: 2.5 m/s SV speed.

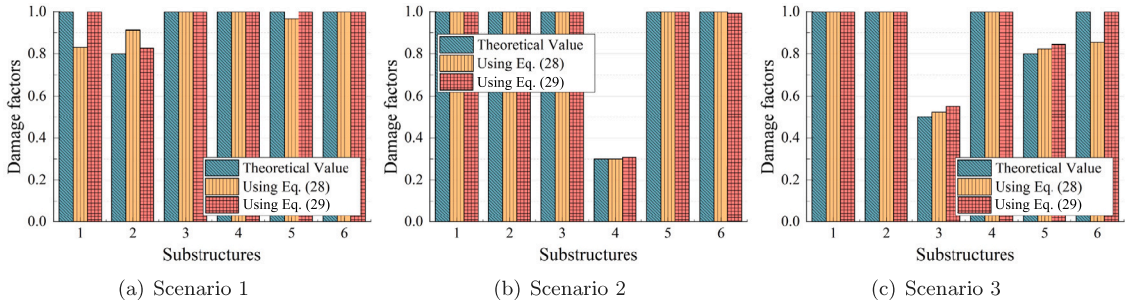

(a) Scenario 1 (b) Scenario 2 (c) Scenario 3

Fig. 12. Damage detection results for different scenarios: 8.3 m/s SV speed.

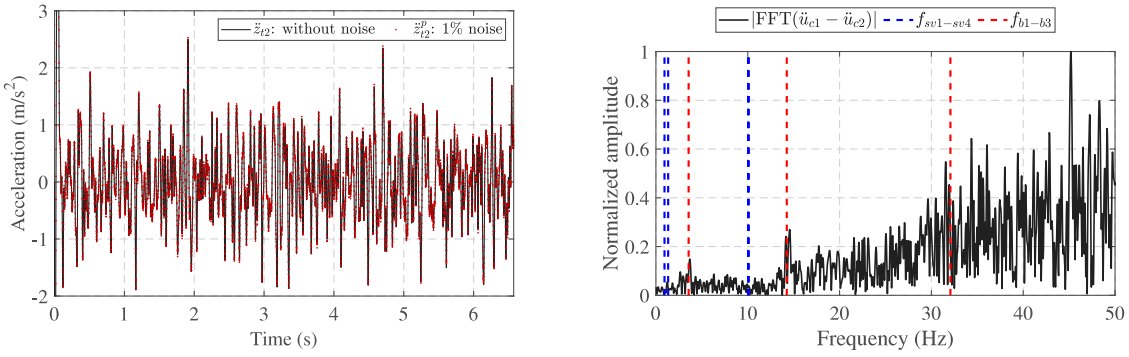

(a) Rear wheel vibrations of the SV (b) Residual CP frequency spectrum (no traffic)

Fig. 13. Indirect bridge frequency identification with 1% noise.

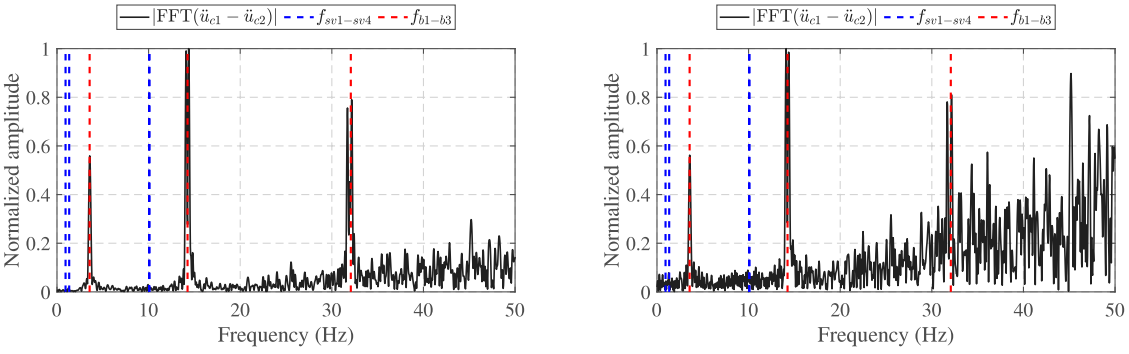

(a) 1% noise (b) 3% noise

Fig. 14. Indirect bridge frequency identification with noise and ongoing traffic.

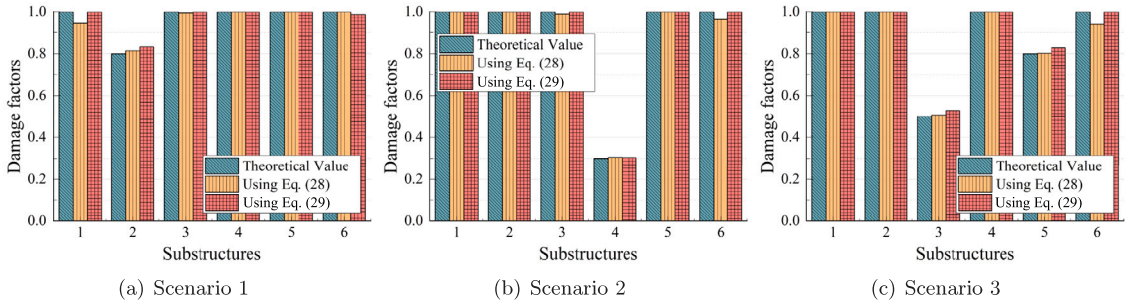

Fig. 15. Damage detection results for different scenarios: 1% noise.

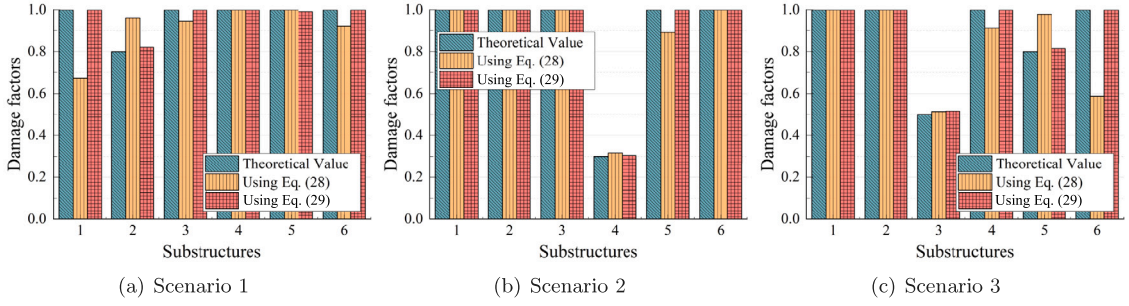

Fig. 16. Damage detection results for different scenarios: 3% noise.

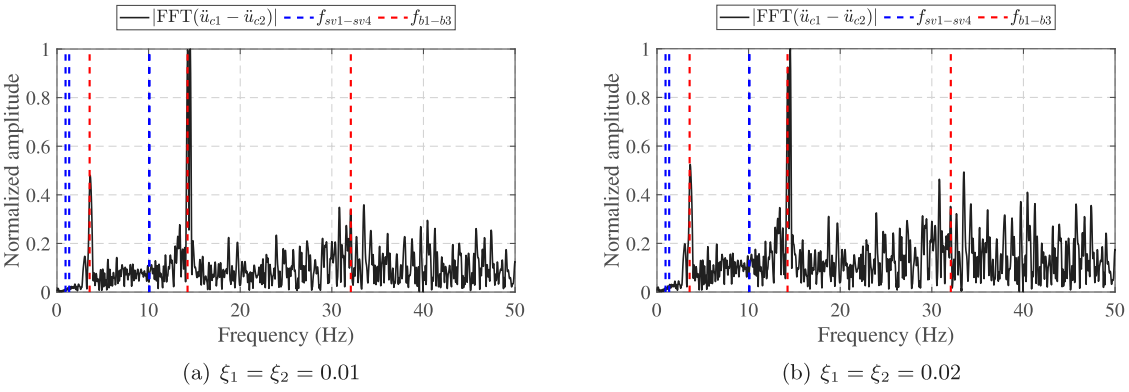

Fig. 17. Indirect bridge frequency identification with different bridge damping.

effects of environmental noise. From Fig. 14, one can also notice that when the noise level is low (say 1% noise), the bridge's frequencies can be identified well. But with the increase in the noise level (say 3% noise), the third frequency becomes overshadowed by the noise, whereas the first two frequencies are still identifiable.

The indirect frequency identification results when the PT is employed at different positions are listed in Table A2 in Appendix B. It can be noticed that low noise levels have little influence on frequency identification. However, larger noise levels can hinder the identification of higher modes. Occasionally, the third bridge frequency is unable to be identified. Nonetheless, this inverse influence only exists for frequencies above 20 Hz. It indicates that the frequency identification results on the first two bridge frequencies will not be affected. In addition, we can see that the noise only has an influence on whether the frequency is identifiable or not in the frequency domain, but it does not change the identified value of frequencies. Therefore, in light of these findings, when the damage detection is performed, K in Fig. 2 is selected as 3 for low noise level but equals 2 for higher noise level. The damage detection results are shown in Figs. 15 and 16.

From Figs. 15 and 16, we can see that when the noise level is low, similar results are obtained as the case study in Section 3.3, and the novel objective function can outperform the traditional one. The position and degree of the damage can be detected despite the environmental noises. When the noise level increases and only the first two bridge frequencies can be utilized, we can see that the Eq. (28) is susceptible to incorrectly identifying the damage location and severity because of the limited modal information, especially for scenarios of minor damage and multiple damages. However, when Eq. (29) is employed, it can effectively locate and quantify the damage in all scenarios even though only two bridge frequencies are employed, which verifies the robustness of the newly proposed objective function.

4.3. Bridge damping

Bridge damping can restrain the bridge's vibration. In other words, the energy transmitted from the vehicle will be consumed by the damping, which, in return, makes less dynamic information transferred to the vehicle. Fig. 17 has plotted the indirect frequency identification results when different damping ratios are considered. We can see that due to the influence of the bridge damping ratio, the third bridge frequency is not outstanding in the frequency domain, although the first two are still identifiable. Similar to resisting the influence of noises, two ongoing

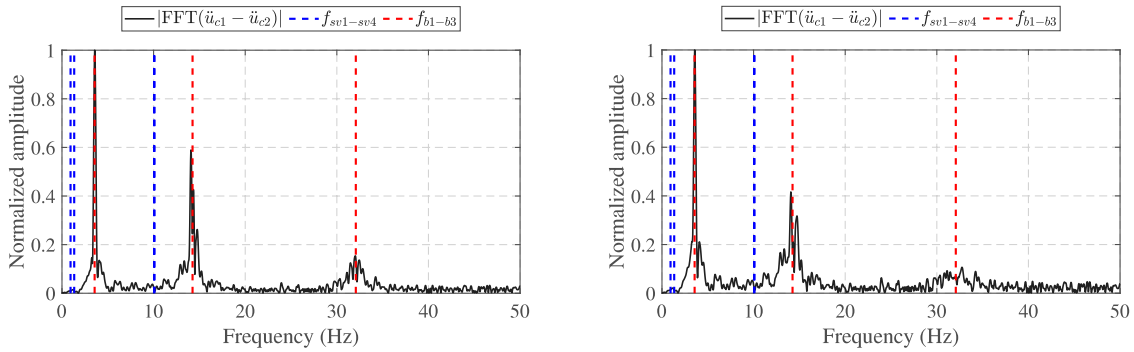

Fig. 18. Indirect bridge frequency identification with bridge damping and ongoing traffic.

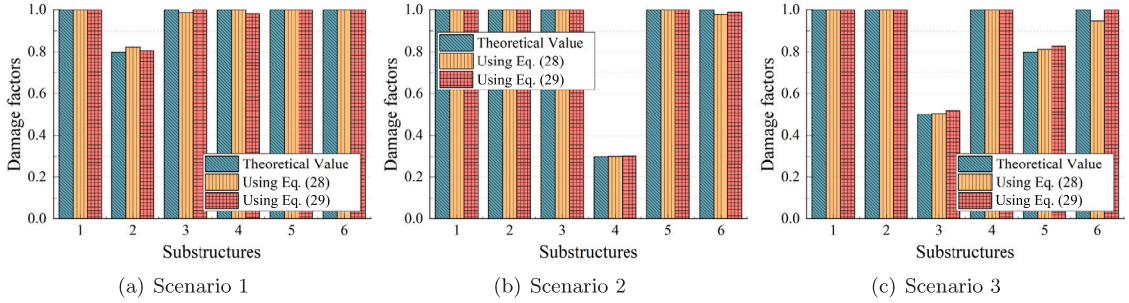

Fig. 19. Damage detection results for different scenarios: $\xi_1=\xi_2=0.01$.

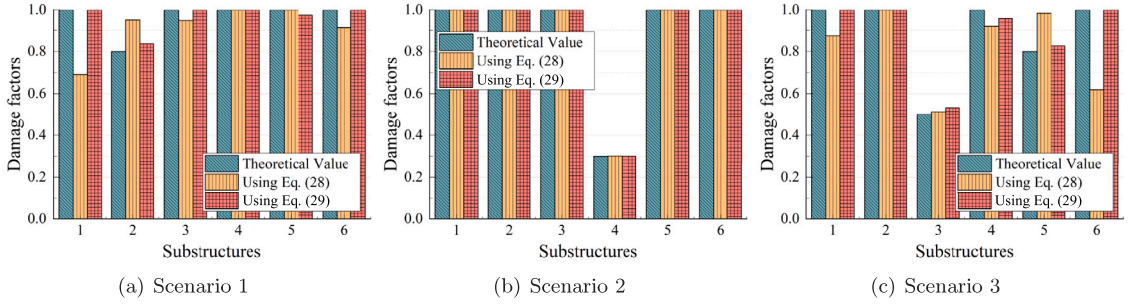

Fig. 20. Damage detection results for different scenarios: $\xi_1=\xi_2=0.02$.

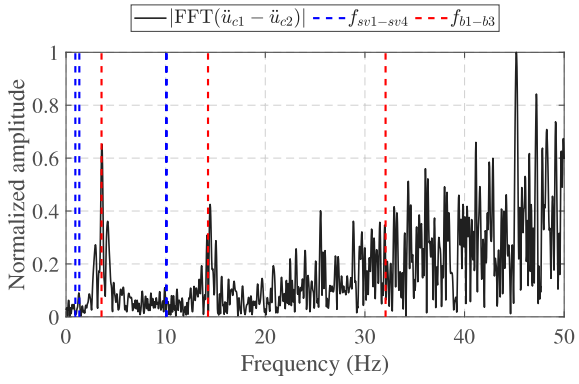

Fig. 21. Indirect bridge frequency identification of the practical case.

traffic vehicles, V1 and V2, are considered. The frequency identification results with ongoing traffic are plotted in Fig. 18. It can be clearly seen that when the damping ratio is low ($\xi_1=\xi_2=0.01$), the bridge's first three frequencies are highlighted and recognizable. But when the damping ratio increases to $\xi_1=\xi_2=0.02$, the third bridge frequency is unidentifiable occasionally (see Fig. 18b). By employing the PT in all locations and performing the indirect frequency identification using residual CP responses, we have listed all frequency values in Table A3 in Appendix B. We can see that when the damping ratio is 0.02 for the first and second modes, the third bridge frequency cannot be identified sometimes, especially for the multiple damage scenario. Under this condition, only the first two bridge frequencies can be utilized for damage detection purposes.

Figs. 19 and 20 have plotted the damage detection results when different damping ratios are considered. It can be seen that low damping ratios have little influence on damage detection accuracy. The location and degree of damage can be identified well. After the damping increases, even though only the first two bridge frequencies are available for damage detection, the damage detection results are still pretty reliable when Eq. (29) is employed. It means that the damping can have an influence on the identification of higher modes but will not

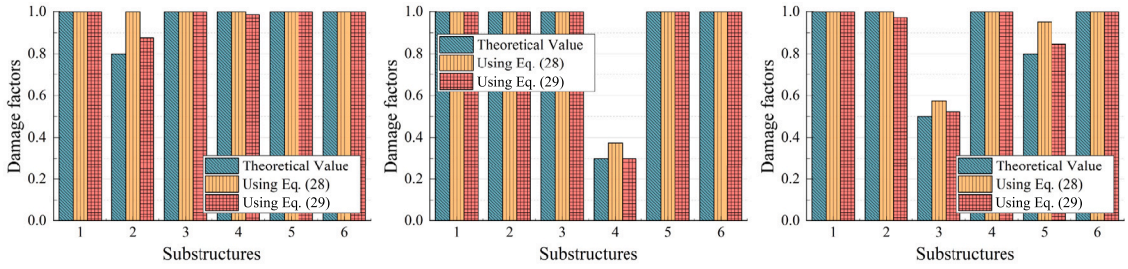

Fig. 22. Damage detection results for different scenarios: the practical case.

Table A1
Identified frequencies with different speeds of the SV (Hz)

Factor		v = 2.5 m/s					v = 8.3 m/s				
PT's position		j = 1	j = 2	j = 3	j = 4	j = 5	j = 1	j = 2	j = 3	j = 4	j = 5
Scenario 1	f_{b1}^j	3.2959	3.2044	3.1433	3.2044	3.2959	3.4180	3.3569	3.0212	3.3569	3.4180
	f_{b2}^j	12.7563	12.7869	13.3057	12.8479	12.7563	12.7258	12.7563	13.2751	12.7869	12.6953
	f_{b3}^j	29.8157	29.3274	29.7546	29.3579	29.7241	29.7241	29.4189	29.6021	29.4495	29.6326
Scenario 2	f_{b1}^j	2.6856	2.5024	2.4109	2.4719	2.5940	2.5940	2.5024	2.4719	2.4719	2.5635
	f_{b2}^j	12.1155	12.1155	12.7258	12.4817	12.3901	12.3291	12.3291	12.6648	12.4512	12.4207
	f_{b3}^j	27.2827	27.0386	27.1301	26.1536	26.7334	27.1912	27.0691	27.1301	26.3977	26.7944
Scenario 3	f_{b1}^j	2.9602	2.8076	2.8076	2.8076	2.9602	3.0517	2.8076	2.6856	2.8076	3.0823
	f_{b2}^j	12.3901	12.3901	12.7258	12.2375	12.0850	12.3901	12.3569	12.6343	12.3901	11.9324
	f_{b3}^j	27.6489	27.2522	28.0151	27.8015	28.2288	27.7710	27.1912	28.1067	27.7100	28.1982

influence the precision of frequency identification very much when the ongoing traffic is considered.

4.4. A more practical case

In the preceding sections, all influence factors are individually analyzed. However, in practical engineering, these factors may positively or negatively affect the proposed damage detection strategy. In this section, the capability of the proposed method is evaluated under the influence of most external factors, such as environmental noise, bridge damping, and ongoing traffics. Here, the environmental noise level is considered higher as 5%, which is more general in practical applications [7]. The damping ratios are assumed as $\xi_1 = \xi_2 = 0.02$. All passing vehicles V1–V4 in Table 3 are regarded as ongoing traffic. The indirect bridge frequency identification results in absence of the PT are shown in Fig. 21. It can be seen that the first two bridge frequencies are still outstanding in the frequency domain despite there being the majority of influence factors, but the third one has been completely submerged. After the moving PT is introduced, the identified bridge frequencies are listed in Table A4 in Appendix B.

Then, the next step entails performing damage detection using the indirectly identified frequency values. An additional issue here is that for the FE model of the bridge, it is typically challenging to construct a precise numerical model in practice. To include this consideration, we assume there are errors when building the FE model. The utilized parameters of the bridge's FE model are as follows: $\hat{L} = 30.5$ m, $\hat{E}_b\hat{I}_b = 2.375 \times 10^{10}$ N/m^2, and $\hat{\bar{m}} = 5800$ kg/m^3, which represents model updating errors of the bridge. When the FE model with errors is utilized, the damage detection results for all three scenarios are shown in Fig. 22.

From Fig. 22, one finds that for the minor damage, when most influence factors are included, Eq. (28) is not able to find the location and degree of the damage but regards all substructures as intact, but it can still identify the single large damage in scenario 2. However, if there are several damage locations and different degrees, it tends to identify the large damage (substructure 3 in scenario 3) but ignore the minor damage (substructure 5 in scenario 3). The above problem can be addressed by Eq. (29). It can be seen that when the MAC-based objective function is utilized, it can identify all damage locations and degrees with acceptable precision, which confirms the effectiveness of the proposed strategy using an SV and PT.

5. Conclusions and future work

This paper proposes an indirect damage detection strategy using the sensing vehicle and temporarily parked truck, in which a novel MAC-based objective function that performs more robustly than the traditional relative error-based one is also included. The CP response from the SV's accelerations is back-calculated to remove the influence of its self-frequencies, and the residual response is then utilized to eliminate the inverse effects of road roughness. Possible positive or negative influence factors are explored and a practical case is investigated to verify the effectiveness of the proposed method. Based on the above analysis, several concluding remarks are drawn below:

(1) The CP response of the SV is derived by considering the damping of suspension and tires simultaneously and errors in installing sensors. Results of numerical simulations have demonstrated the effectiveness of CP response calculation, and the employed residual CP response can eliminate the influence of the vehicle itself and road roughness, making the bridge frequencies more outstanding and identifiable.
(2) By introducing the PT to different locations, more modal information about the bridge is obtained, and its sensitivity to local damage is enhanced. After the combination of different bridge modes and the new objective function, the proposed method can be performed robustly despite acceptable errors in indirectly identifying bridge frequencies.
(3) Higher speeds of the sensing vehicle will decrease the frequency resolution, causing poor indirect bridge frequency identification thus negatively affecting the damage detection.
(4) Ongoing traffic plays a "positive" role in resisting the overshadowing effects of environmental noises and bridge damping in the high-frequency range thus is helpful for damage detection by providing modal information about higher modes of the bridge.

Table A2
Identified frequencies with different noise levels (Hz)

Factor		E_p = 1%					E_p = 3%				
PT's position		$j=1$	$j=2$	$j=3$	$j=4$	$j=5$	$j=1$	$j=2$	$j=3$	$j=4$	$j=5$
Scenario 1	f_{b1}^j	3.3569	3.1738	3.1128	3.2044	3.3569	3.3569	3.1738	3.1128	3.2044	3.3569
	f_{b2}^j	12.7563	12.8174	13.3057	12.8479	12.7258	12.7563	12.8174	13.3057	12.8479	12.7258
	f_{b3}^j	29.7852	29.3884	29.7241	29.3579	29.6936	–	29.3884	–	29.3579	–
Scenario 2	f_{b1}^j	2.6550	2.5024	2.4109	2.4719	2.6245	2.6550	2.5024	2.4109	2.4719	2.6245
	f_{b2}^j	12.2070	12.1460	12.6648	12.4817	12.4207	12.2070	12.1460	12.6648	12.4817	12.4207
	f_{b3}^j	27.2522	27.0691	27.1301	26.1536	26.7334	27.2522	27.0691	27.1301	–	26.7334
Scenario 3	f_{b1}^j	2.9602	2.8076	2.7466	2.8076	2.9602	2.9602	2.8076	2.7466	2.8076	2.9602
	f_{b2}^j	12.3596	12.2986	12.6343	12.2375	12.0544	12.3596	12.2986	12.6343	12.2375	12.0544
	f_{b3}^j	27.6489	27.2217	28.0151	27.8625	28.2593	27.6489	27.2217	28.0151	–	28.2593

Table A3
Identified frequencies with different damping ratios (Hz)

Factor		$\xi_1=\xi_2$ = 0.01					$\xi_1=\xi_2$ = 0.02				
PT's position		$j=1$	$j=2$	$j=3$	$j=4$	$j=5$	$j=1$	$j=2$	$j=3$	$j=4$	$j=5$
Scenario 1	f_{b1}^j	3.3569	3.1738	3.1128	3.2044	3.3569	3.3569	3.1738	3.1128	3.2044	3.3569
	f_{b2}^j	12.8784	12.8784	13.3057	12.8784	12.7563	12.7563	12.7869	13.3057	12.8784	12.7258
	f_{b3}^j	30.0903	29.4495	29.9072	29.4495	29.9072	30.1208	–	29.9072	–	29.9377
Scenario 2	f_{b1}^j	2.6550	2.5024	2.4109	2.4414	2.6245	2.6550	2.5024	2.4109	2.4414	2.6245
	f_{b2}^j	12.2986	12.2681	12.5732	12.5427	12.4207	12.2375	12.2375	12.6648	12.4521	12.4521
	f_{b3}^j	27.1301	27.1301	27.1301	26.2756	26.7029	–	–	–	26.3062	–
Scenario 3	f_{b1}^j	2.9602	2.8076	2.7466	2.8076	2.9602	2.9602	2.8076	2.7466	2.8076	2.9602
	f_{b2}^j	12.4207	12.2986	12.7258	12.2375	12.0544	12.3291	12.2986	12.6343	12.2375	12.0850
	f_{b3}^j	27.7405	27.2827	28.0151	27.8625	28.2593	–	–	–	–	–

Table A4
Identified frequencies in a more practical case (Hz)

PT's position		$j=1$	$j=2$	$j=3$	$j=4$	$j=5$
Scenario 1	f_{b1}^j	3.3264	3.1433	3.1128	3.1738	3.3264
	f_{b2}^j	12.7563	12.7563	13.3057	12.8784	12.7258
Scenario 2	f_{b1}^j	2.7466	2.5024	2.4109	2.4719	2.6550
	f_{b2}^j	12.1155	12.1155	12.7563	12.7563	12.7563
Scenario 3	f_{b1}^j	2.9297	2.8076	2.7771	2.8076	2.9297
	f_{b2}^j	12.3291	12.2681	12.7563	12.0850	12.0850

(5) For a more practical case considering most influence factors and model updating errors, the proposed MAC-based objective function can detect the bridge's damage position and degree robustly with acceptable precision.

Despite interesting findings in this paper, several influencing factors, such as engine effects, temperature variations, winds, and earthquakes, deserve further investigation. In addition, in the bridge damage detection process, this work typically utilized indirectly identified bridge frequencies. The effectiveness of the modal shape, as another important modal parameter that can be retrieved from vehicle responses, for damage detection will be checked in our future studies. The proposed approaches will be explored and examined in field tests before engineering applications.

CRediT authorship contribution statement

Zhenkun Li: Conceptualization, Software, Formal analysis, Methodology, Writing – original draft, Editing. **Yifu Lan:** Writing – review & editing. **Weiwei Lin:** Funding acquisition, Supervision, Writing – review & editing.

Declaration of competing interest

The authors declare the following financial interests/personal relationships which may be considered as potential competing interests: Weiwei Lin reports financial support was provided by Jane and Aatos Erkko Foundation. Yifu Lan reports financial support was provided by Finnish Foundation for Technology Promotion (TES). Yifu Lan reports financial support was provided by Chinese Scholarship Council (CSC).

Data availability

Data will be made available on request.

Acknowledgments

This research is financially sponsored by the Jane and Aatos Erkko Foundation in Finland (Decision number: 210018). Y. Lan is also financially supported by the Finnish Foundation for Technology Promotion (TES) and Chinese Scholarship Council (CSC).

Appendix A

$$\mathbf{M}_{sv}=\begin{bmatrix} m_v & 0 & 0 & 0 \\ 0 & I_v & 0 & 0 \\ 0 & 0 & m_{t1} & 0 \\ 0 & 0 & 0 & m_{t2} \end{bmatrix}$$

$$\mathbf{C}_{sv}=\begin{bmatrix} c_{s1}+c_{s2} & a_1c_{s1}-a_2c_{s2} & -c_{s1} & -c_{s2} \\ a_1c_{s1}-a_2c_{s2} & a_1^2c_{s1}+a_2^2c_{s2} & -a_1c_{s1} & a_2c_{s2} \\ -c_{s1} & -a_1c_{s1} & c_{s1}+c_{t1} & 0 \\ -c_{s2} & a_2c_{s2} & 0 & c_{s2}+c_{t2} \end{bmatrix}$$

$$\mathbf{K}_{sv}=\begin{bmatrix} k_{s1}+k_{s2} & a_1k_{s1}-a_2k_{s2} & -k_{s1} & -k_{s2} \\ a_1k_{s1}-a_2k_{s2} & a_1^2k_{s1}+a_2^2k_{s2} & -a_1k_{s1} & a_2k_{s2} \\ -k_{s1} & -a_1k_{s1} & k_{s1}+k_{t1} & 0 \\ -k_{s2} & a_2k_{s2} & 0 & k_{s2}+k_{t2} \end{bmatrix}$$

Appendix B

See Tables A1–A4

References

[1] Sun L, Shang Z, Xia Y, Bhowmick S, Nagarajaiah S. Review of bridge structural health monitoring aided by big data and artificial intelligence: From condition assessment to damage detection. J Struct Eng 2020;146(5):04020073. http://dx.doi.org/10.1061/(ASCE)ST.1943-541X.0002535.

[2] An Y, Chatzi E, Sim S-H, Laflamme S, Blachowski B, Ou J. Recent progress and future trends on damage identification methods for bridge structures. Struct Control Health Monit 2019;26(10):e2416. http://dx.doi.org/10.1002/stc.2416.

[3] Hao H, Bi K, Chen W, Pham TM, Li J. Towards next generation design of sustainable, durable, multi-hazard resistant, resilient, and smart civil engineering structures. Eng Struct 2023;277:115477. http://dx.doi.org/10.1016/j.engstruct.2022.115477.

[4] Farrar CR, Worden K. An introduction to structural health monitoring. Phil Trans R Soc A 2007;365(1851):303–15. http://dx.doi.org/10.1098/rsta.2006.1928.

[5] Bao Y, Chen Z, Wei S, Xu Y, Tang Z, Li H. The state of the art of data science and engineering in structural health monitoring. Engineering 2019;5(2):234–42. http://dx.doi.org/10.1016/j.eng.2018.11.027.

[6] Spencer BF, Hoskere V, Narazaki Y. Advances in computer vision-based civil infrastructure inspection and monitoring. Engineering 2019;5(2):199–222. http://dx.doi.org/10.1016/j.eng.2018.11.030.

[7] Xu H, Liu YH, Wang ZL, Shi K, Zhang B, Yang YB. General contact response of single-axle two-mass test vehicles for scanning bridge frequencies considering suspension effect. Eng Struct 2022;270:114880. http://dx.doi.org/10.1016/j.engstruct.2022.114880.

[8] Yang YB, Lin CW, Yau JD. Extracting bridge frequencies from the dynamic response of a passing vehicle. J Sound Vib 2004;272(3–5):471–93. http://dx.doi.org/10.1016/S0022-460X(03)00378-X.

[9] Lin CW, Yang YB. Use of a passing vehicle to scan the fundamental bridge frequencies: An experimental verification. Eng Struct 2005;27(13):1865–78. http://dx.doi.org/10.1016/j.engstruct.2005.06.016.

[10] Wang ZL, Yang JP, Shi K, Xu H, Qiu FQ, Yang YB. Recent advances in researches on vehicle scanning method for bridges. Int J Struct Stab Dyn 2022;22(15):2230005. http://dx.doi.org/10.1142/S0219455422300051.

[11] Malekjafarian A, Corbally R, Gong W. A review of mobile sensing of bridges using moving vehicles: Progress to date, challenges and future trends. Structures 2022;44:1466–89. http://dx.doi.org/10.1016/j.istruc.2022.08.075.

[12] European Commission, Joint Research Centre, Gkoumas K, Galassi M, Allaix D, Anthoine A, et al. Indirect structural health monitoring (iSHM) of transport infrastructure in the digital age : MITICA (monitoring transport infrastructures with connected and automated vehicles) workshop report. Publications Office of the European Union; 2023, http://dx.doi.org/10.2760/364830.

[13] Zhou J, Lu Z, Zhou Z, Pan C, Cao S, Cheng J, et al. Extraction of bridge mode shapes from the response of a two-axle passing vehicle using a two-peak spectrum idealized filter approach. Mech Syst Signal Process 2023;190:110122. http://dx.doi.org/10.1016/j.ymssp.2023.110122.

[14] González A, Obrien EJ, McGetrick PJ. Identification of damping in a bridge using a moving instrumented vehicle. J Sound Vib 2012;331(18):4115–31. http://dx.doi.org/10.1016/j.jsv.2012.04.019.

[15] Feng K, Casero M, González A. Characterization of the road profile and the rotational stiffness of supports in a bridge based on axle accelerations of a crossing vehicle. Comput-Aided Civ Infrastruct Eng 2023;1–20. http://dx.doi.org/10.1111/mice.12974.

[16] Yang YB, Chang KC, Li YC. Filtering techniques for extracting bridge frequencies from a test vehicle moving over the bridge. Eng Struct 2013;48:353–62. http://dx.doi.org/10.1016/j.engstruct.2012.09.025.

[17] Yang YB, Chang KC. Extraction of bridge frequencies from the dynamic response of a passing vehicle enhanced by the EMD technique. J Sound Vib 2009;322(4–5):718–39. http://dx.doi.org/10.1016/j.jsv.2008.11.028.

[18] OBrien EJ, Malekjafarian A, González A, O'brien E, Malekjafarian A, González A. Application of empirical mode decomposition to drive-by bridge damage detection. Eur J Mech A 2017;61:151–63. http://dx.doi.org/10.1016/j.euromechsol.2016.09.009.

[19] Sadeghi Eshkevari S, Matarazzo TJ, Pakzad SN. Bridge modal identification using acceleration measurements within moving vehicles. Mech Syst Signal Process 2020;141:106733. http://dx.doi.org/10.1016/j.ymssp.2020.106733.

[20] Locke W, Redmond L, Schmid M. Evaluating OMA system identification techniques for drive-by health monitoring on short span bridges. J Bridge Eng 2022;27(9):04022079. http://dx.doi.org/10.1061/(ASCE)BE.1943-5592.0001923.

[21] Yang YB, Zhang B, Qian Y, Wu Y. Contact-point response for modal identification of bridges by a moving test vehicle. Int J Struct Stab Dyn 2018;18(5):1850073. http://dx.doi.org/10.1142/S0219455418500736.

[22] Nayek R, Narasimhan S. Extraction of contact-point response in indirect bridge health monitoring using an input estimation approach. J Civ Struct Health Monit 2020;10:815–31. http://dx.doi.org/10.1007/s13349-020-00418-z.

[23] Corbally R, Malekjafarian A. A data-driven approach for drive-by damage detection in bridges considering the influence of temperature change. Eng Struct 2022;253:113783. http://dx.doi.org/10.1016/j.engstruct.2021.113783.

[24] Xu H, Liu YH, Yang M, Yang DS, Yang YB. Scanning and separating vertical and torsional–flexural frequencies of thin-walled girder bridges by a single-axle test vehicle. Thin-Walled Struct 2023;182:110266. http://dx.doi.org/10.1016/j.tws.2022.110266.

[25] Kong X, Cai CS, Kong B. Numerically extracting bridge modal properties from dynamic responses of moving vehicles. J Eng Mech 2016;142(6):04016025. http://dx.doi.org/10.1061/(asce)em.1943-7889.0001033.

[26] Yang YB, Li YC, Chang KC. Using two connected vehicles to measure the frequencies of bridges with rough surface: A theoretical study. Acta Mech 2012;223(8):1851–61. http://dx.doi.org/10.1007/s00707-012-0671-7.

[27] Shi K, Mo XQ, Xu H, Wang ZL, Hu XS, Yang YB. Furthering extraction of torsional–flexural frequencies for thin-wall beams from the rocking motion of a two-wheel test vehicle. Thin-Walled Struct 2022;175:109224. http://dx.doi.org/10.1016/j.tws.2022.109224.

[28] Yang YB, Mo XQ, Shi K, Wang ZL, Xu H, Wu YT. Contact residue for simultaneous removal of vehicle's frequency and surface roughness in scanning bridge frequencies using two connected vehicles. Int J Struct Stab Dyn 2021;21(13):2171006. http://dx.doi.org/10.1142/S0219455421710061.

[29] He Y, Yang JP. Using acceleration residual spectrum from single two-axle vehicle at contact points to extract bridge frequencies. Eng Struct 2022;266:114538. http://dx.doi.org/10.1016/j.engstruct.2022.114538.

[30] Yang YB, Xu H, Wang ZL, Shi K. Using vehicle–bridge contact spectra and residue to scan bridge's modal properties with vehicle frequencies and road roughness eliminated. Struct Control Health Monit 2022;29(8):e2968. http://dx.doi.org/10.1002/stc.2968.

[31] Yang YB, Wang ZL, Yao H, Zhang B, Xu H, Shi K. Weak-end and frequency detection of elastically supported bridges by contact residual response of two-axle test vehicle in a round trip. J Bridge Eng 2023;28(3):06023001. http://dx.doi.org/10.1061/JBENF2.BEENG-5952.

[32] Hou J, Li Z, Zhang Q, Jankowski Ł, Zhang H. Local mass addition and data fusion for structural damage identification using approximate models. Int J Struct Stab Dyn 2020;20(11):2050124. http://dx.doi.org/10.1142/S0219455420501242.

[33] Xu YL, Chen J. Structural damage detection using empirical mode decomposition: Experimental investigation. J Eng Mech 2004;130(11):1279–88. http://dx.doi.org/10.1061/(ASCE)0733-9399(2004)130:11(1279).

[34] Li J, Zhu X, Guo J. Bridge modal identification based on successive variational mode decomposition using a moving test vehicle. Adv Struct Eng 2022;25(11):2284–300. http://dx.doi.org/10.1177/13694332221092678.

[35] Bayissa WL, Haritos N, Thelandersson S. Vibration-based structural damage identification using wavelet transform. Mech Syst Signal Process 2008;22(5):1194–215. http://dx.doi.org/10.1016/j.ymssp.2007.11.001.

[36] Lan Y, Zhang Y, Lin W. Diagnosis algorithms for indirect bridge health monitoring via an optimized AdaBoost-linear SVM. Eng Struct 2023;275:115239. http://dx.doi.org/10.1016/j.engstruct.2022.115239.

[37] Li Z, Lin W, Zhang Y. Real-time drive-by bridge damage detection using deep auto-encoder. Structures 2023;47:1167–81. http://dx.doi.org/10.1016/j.istruc.2022.11.094.

[38] Yang J-H, Lam H-F, An Y-H. Development of a two-phase adaptive MCMC method for efficient Bayesian model updating of complex dynamic systems. Eng Struct 2022;270:114836. http://dx.doi.org/10.1016/j.engstruct.2022.114836.

[39] Cong S, Hu S-LJ, Li H-J. FRF-based pole-zero method for finite element model updating. Mech Syst Signal Process 2022;177:109206. http://dx.doi.org/10.1016/j.ymssp.2022.109206.

[40] Jaishi B, Ren W-X. Damage detection by finite element model updating using modal flexibility residual. J Sound Vib 2006;290(1–2):369–87. http://dx.doi.org/10.1016/j.jsv.2005.04.006.

[41] Khatir S, Wahab MA, Boutchicha D, Khatir T. Structural health monitoring using modal strain energy damage indicator coupled with teaching-learning-based optimization algorithm and isogoemetric analysis. J Sound Vib 2019;448:230–46. http://dx.doi.org/10.1016/j.jsv.2019.02.017.

[42] Hou J, Li C, Jankowski Ł, Shi Y, Su L, Yu S, et al. Damage identification of suspender cables by adding virtual supports with the substructure isolation method. Struct Control Health Monit 2021;28(3):e2677. http://dx.doi.org/10.1002/stc.2677.

[43] Chang KC, Kim CW, Borjigin S. Variability in bridge frequency induced by a parked vehicle. Smart Struct Syst 2014;13(5):755–73. http://dx.doi.org/10.12989/sss.2014.13.5.755.

[44] He W-Y, Ren W-X. Structural damage detection using a parked vehicle induced frequency variation. Eng Struct 2018;170:34–41. http://dx.doi.org/10.1016/j.engstruct.2018.05.082.

[45] Cao L, He W-Y, Ren W-X. Damage localization and quantification for beam bridges based on frequency variation of parked vehicle-bridge systems. Structures 2021;31:357–68. http://dx.doi.org/10.1016/j.istruc.2021.01.098.

[46] He W-Y, Ren W-X, Zuo X-H. Mass-normalized mode shape identification method for bridge structures using parking vehicle-induced frequency change. Struct Control Health Monit 2018;25(6):e2174. http://dx.doi.org/10.1002/stc.2174.

[47] Locke W, Sybrandt J, Redmond L, Safro I, Atamturktur S. Using drive-by health monitoring to detect bridge damage considering environmental and operational effects. J Sound Vib 2020;468:115088. http://dx.doi.org/10.1016/j.jsv.2019.115088.

[48] ISO 8608. Mechanical vibration-road surface profiles-reporting of measured data. 2nd ed. (2016-11-01). Geneva: International Organization for Standardization; 2016.
[49] Yang YB, Wang B, Wang Z, Shi K, Xu H. Scanning of bridge surface roughness from two-axle vehicle response by EKF-UI and contact residual: Theoretical study. Sensors 2022;22(9):3410. http://dx.doi.org/10.3390/s22093410.
[50] Zhang Q, Hou J, An X, Jankowski Łukasz, Duan Z, Hu X. Vehicle parameter identification based on vehicle frequency response function. J Sound Vib 2023;542:117375. http://dx.doi.org/10.1016/j.jsv.2022.117375.
[51] Hou J, Li Z, Jankowski Ł, Wang S. Estimation of virtual masses for structural damage identification. Struct Control Health Monit 2020;27(8):e2585. http://dx.doi.org/10.1002/stc.2585.
[52] Zhou X, Kim C-W, Zhang F-L, Chang K-C. Vibration-based Bayesian model updating of an actual steel truss bridge subjected to incremental damage. Eng Struct 2022;260:114226. http://dx.doi.org/10.1016/j.engstruct.2022.114226.
[53] Hou R, Xia Y, Bao Y, Zhou X. Selection of regularization parameter for l1-regularized damage detection. J Sound Vib 2018;423:141–60. http://dx.doi.org/10.1016/j.jsv.2018.02.064.
[54] Zhou X-Q, Xia Y, Weng S. L1 regularization approach to structural damage detection using frequency data. Struct Health Monit 2015;14(6):571–82. http://dx.doi.org/10.1177/1475921715604386.
[55] Jazar RN. Vehicle dynamics, vol. 1, Springer; 2008.
[56] Jian X, Xia Y, Sun L. Indirect identification of bridge frequencies using a four-wheel vehicle: Theory and three-dimensional simulation. Mech Syst Signal Process 2022;177:109155. http://dx.doi.org/10.1016/j.ymssp.2022.109155.
[57] Li J, Zhu X, Law S-S, Samali B. A two-step drive-by bridge damage detection using dual Kalman filter. Int J Struct Stab Dyn 2020;20(10):2042006. http://dx.doi.org/10.1142/S0219455420420067.
[58] Shi Z, Uddin N. Extracting multiple bridge frequencies from test vehicle — A theoretical study. J Sound Vib 2021;490:115735. http://dx.doi.org/10.1016/J.JSV.2020.115735.
[59] Yang YB, Xu H, Mo XQ, Wang ZL, Wu YT. An effective procedure for extracting the first few bridge frequencies from a test vehicle. Acta Mech 2021;232(3):1227–51. http://dx.doi.org/10.1007/s00707-020-02870-w.